Chapter 3

Phytochemical investigation of *Dysoxylum malabaricum* Bedd. bark using LC-MS-based dereplication strategy and cytotoxic evaluation

3. Phytochemical investigation of *Dysoxylum malabaricum* Bedd. bark using LC-MS-based dereplication strategy and cytotoxic evaluation

3.1 Literature review

The crude extract from biological sources comprises thousands of structurally diverse compounds, often existing across a broad spectrum of concentrations [31]. The process of isolating these compounds from each other, particularly when many are present in limited quantities, poses a considerable challenge. Also, exploring the bioactivity of phytochemicals and uncovering new compounds within the vast, diverse plant species demands the development of a reliable and effective methodology [32]. Therefore, the dereplication strategy is one of the best methods for the rapid identification of metabolites from the crude mixture [33, 34]. It prompts the identification of known metabolites present in crude extracts or fractions, which overcomes expensive and time-consuming isolation and structure elucidation procedures [35, 36]. Typically, the dereplication strategy relies on matching molecular features found in unknown compounds, whether through spectroscopic/spectrometric or structural means, with data archived in spectroscopic databases as well as structural databases [37]. Following an initial screening of extracts, a dereplication strategy is commonly used. Among the most prevalent techniques are hyphenated methods, where LC-MS is most extensively used in natural product drug discovery. This technique allows the analysis of spectra obtained, thereby furnishing structural information about the compounds within mixtures. LC-MS-based dereplication studies on crude mixtures target new metabolites at the earliest stage [38]. In dereplication investigations, access to a comprehensive database is crucial for effectively analyzing molecular characteristics. The mass spectrometric like LC-MS-derived information used in the chemical database is a regular practice, mainly in proteomics studies [39]. A comprehensive database exclusively for natural products is

required to sort the metabolites based on the taxonomic classification, physicochemical, and spectral properties. The dictionary of natural products is a widely used database containing more than 300000 natural products. It provides access to the biological source (taxonomic classification), chemical (molecular weight, molecular formula, chemical classification, etc.), physical (UV, melting point, boiling point, etc.), and complete or sub-structural information of natural products. The mass information (obtained via LC-MS and HRMS), in conjunction with mutually supportive data such as retention time (t_R), UV/vis, ^{1}H NMR spectra, and substructure search through database mining, aids in accurately identifying metabolites [40-42]. HRMS (High-resolution mass spectrometry) techniques enhance the dereplication process by enabling the prediction of molecular formulas [43]. By analyzing the isotopic distribution patterns of parent ions and their daughter ions, HRMS can suggest likely molecular formulas, aiding in the identification of fragmentation processes from parent to daughter ions [44]. This approach provides valuable insights into the chemical composition and structure of metabolites, thereby streamlining the dereplication process for the identification of new natural products.

Further isolation and structure elucidation are done to confirm the targeted metabolite. The structure elucidation of complex natural products incorporates extensive spectral analytical techniques to determine the structure of the metabolites [45]. The techniques mostly embedded in structural elucidation are LC-MS, HRMS, NMR, infrared spectra, electronic circular dichroism (ECD) spectroscopy, etc. LC-MS serves as an essential tool in assessing the molecular mass and purity of isolated metabolites. HRMS data analysis plays a crucial role in determining the molecular formula and anticipated structure of these metabolites [46]. Further confirmation of these predicted structures is attained through analysis of NMR spectroscopic data. NMR spectroscopy encompasses various techniques such as proton NMR (^{1}H NMR), and carbon NMR (^{13}C NMR), as well as

multidimensional methods like COSY (Correlation Spectroscopy), HSQC (Heteronuclear Single Quantum Coherence), HMBC (Heteronuclear Multiple Bond Correlation) and NOESY (Nuclear Overhauser Effect Spectroscopy) [47-49]. To define the absolute configuration and complete stereochemistry of the natural product of interest ECD experiments are conducted [50-53]. The current study is focused on establishing a DNP-based strategic dereplication platform where the taxonomic, chemical classification, and spectroscopic information acquired by LC-MS and ^{1}H NMR are applied for rapid identification of known metabolites so that a new structure can be targeted for isolation and structural elucidation from plant *Dysoxylum malabaricum (D. malabaricum)*.

The genus *Dysoxylum* belongs to a medicinally important plant family, mahogany (Meliaceae), comprising approximately 80 species predominantly found in Southeast Asia and Australia. *D. malabaricum,* one of the plants from this genus, is an economically significant species endemic to the Western Ghats of India [54]. Biologically active compounds were identified from stems, leaves, and bark of various species of *Dysoxylum* [55]. Phytochemical investigation of *Dysoxylum* has not only identified triterpenoids but also a range of compounds incorporating sesquiterpenoids, diterpenoids, glycosides, tetranortriterpenoid or limonoids, steroids, and alkaloids [56-59]. Triterpenoids, derived from isopentenyl pyrophosphate oligomers, represent predominant phytochemicals in this particular species. The exploration of triterpenoids from *Dysoxylum* dates back to 1976, marked by the discovery of tetranortriterpenoids or limonoids, notably dysobinin, extracted from the fruit of *D. binectariferum* [60]. Also, various chemically diverse triterpenoid skeletons are found in the genus *Dysoxylum viz* tricullane [61], nortriterpenoid, cycloartane, oleanane, euphane, lupane, glabretal and dammarane type [62-65] (Figure 3.1). These eight classes of triterpenoids possess extensive biological functions [66-68].

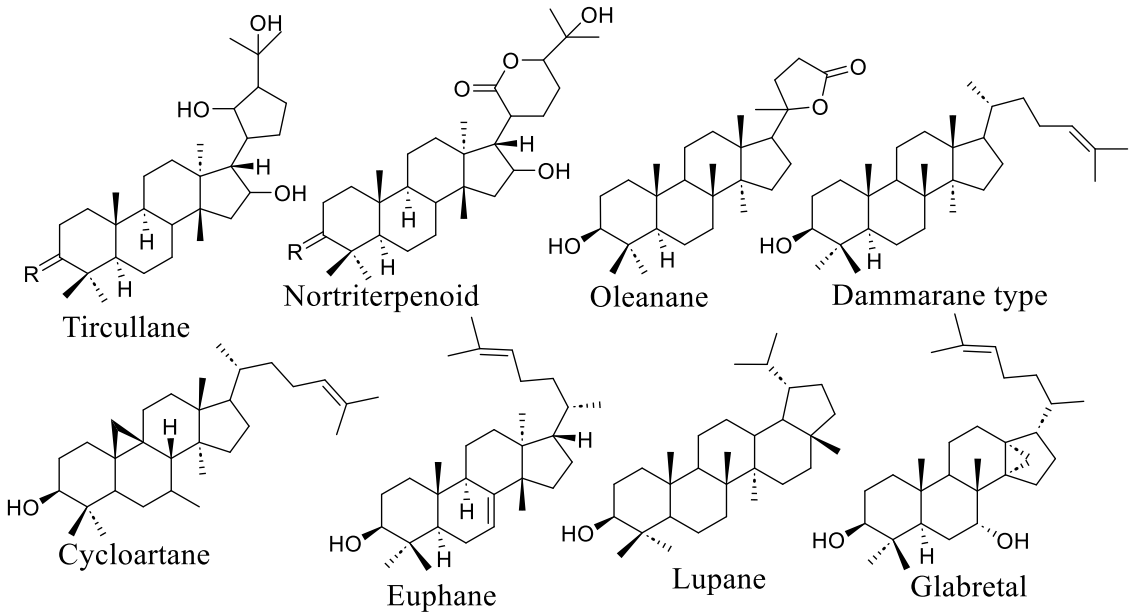

Figure 3.1. Common triterpenoid skeleton found in the phytoconstituents of *Dysoxylum* genus.

The phytoconstituents having different triterpenoid skeletons extracted from the *Dysoxylum* genus are known for their pharmacological potency showcasing activity like anti-inflammatory [69-71], antimalarial, antitumor, cytotoxic, antifeedant, antidepressant, and antimicrobial activity [72-76]. Traditionally, *Dysoxylum* was used in the treatment of diseases like fish poisoning and also possesses antiperiodic, anthelmintic, and emmenagogue properties. Previous research has indicated that the majority of aches, pains, digestive ailments, and lung haemorrhages can be alleviated by consuming a liquid infusion of sliced leaves of *D. gaudichaudianum.* Another study reports the traditional use of *D. binectariferum* for the treatment of leprosy and severe ulcers by indigenous Asians. People in northeast India have used a decoction from *D. gotadhora* and *D. hamiltonii* leaves to address stomachaches, diarrhea, and dysentery. Also, phytochemical investigation of *D. binectariferum* has resulted in the isolation of medicinally important alkaloids. It has been identified as an alternative source for the isolation of rohitukine and camptothecin [77-79]. The alkaloid rohitukine inspired the discovery of clinical drug candidates, flavopiridol and riviciclib, showing CDK inhibitory

action against lymphocytic leukemia. Several derivatives were synthesized to tackle the bioavailability concerns related to the rohitukine basic structure. Among these, IIM-290 exhibited potent inhibition of CDK-9, and bioavailability was enhanced to 71%. IIM-290 is currently in clinical trials for potential cancer treatment [80-83]. *D. binectariferum* is phylogenetically connected to the Ayurvedic plant *D. malabaricum,* primarily used in the treatment of rheumatoid arthritis. However, the phytoconstituents present in the stem, bark, leaves, and fruits of *D. malabaricum* have been little explored till now [84-86].

As per the chemosystematics, common phylogenetic relationships, chemical profiles, and metabolic pathways exist within the plants that belong to the same genus. Since *Dysoxylum malabaricum* and *Dysoxylum binectariferum* are taxonomically related to each other, they may share similar biosynthetic pathways and metabolic processes, suggesting the presence of analogue bioactive compounds. Moreover, the DNP database lists over 380 secondary metabolites; among them, 200 are chemically diverse triterpenoids in the genus *Dysoxylum*. Only six metabolites are reported from *D. malabaricum*, and three of them are triterpenoids. To date, few studies have been conducted on *Dysoxylum malabaricum,* and only two studies have been done on the bark of this species. Given the varied phytochemical attributes of this genus and in our pursuit of identifying bioactive lead molecules, a comprehensive study of this species was planned. This study involves bioassay-guided fractionation and LC-MS DNP-based dereplication to target the new compounds and further explore their cytotoxic evaluation against cancer cell lines.

3.2. Experimental section

3.2.1. General experimental procedures

All chemicals were purchased from Sigma Aldrich and used as received and chromatographic purifications were performed on silica gel (#60−120 or #100−200)

obtained from Merck. The thin-layer chromatography (TLC) was performed on pre-coated silica gel 60 GF_{254} aluminum sheets obtained from Merck and visualized under UV light (254 nm) and by spraying an anisaldehyde−sulfuric acid reagent followed by heating.

The 1D and 2D NMR spectra were recorded on a Bruker-Avance III HD 500 MHz NMR spectrometer using tetramethylsilane (TMS) as the internal standard and are referenced to the residual proton/carbon in the NMR solvent ($CDCl_3$, 7.26/77.1 ppm; CD_3OD, 4.89, 3.30/49.0 ppm, DMSO-d_6, 2.50/39.5 ppm). ESI-MS and HRMS spectra were recorded on Agilent 1100LC-QTOF and HRMS-6540-UHD spectrometers. Molecular weight was determined on an LC-MS instrument equipped with UV and MS detectors (LCMS-2020, Shimadzu, Japan) using an RP column (C_{18}, 3 μm, 150 × 4.6 mm, Thermo Scientific). The solvent system used contains acetonitrile and 0.1% aqueous formic acid in water with a total run time of 30 min. The flow rate of 1 mL/min, detection at 254 nm, and injection volume of 10 μL were the other parameters used here. Semi-preparative HPLC was performed on a Prominence system (Shimadzu) with a UV detector using an RP column (C_{18}, 5 μm, 250 × 1.0 mm, Phenomenex), solvents: acetonitrile and 0.1% aqueous acetic acid in water. The isocratic gradient system was used with a total run time of 60 min, Flow rate of 1 mL/min, detection at 254 nm, and injection volume of 30 μL were used. HPLC systems were controlled by LabSolutions® software (Shimadzu) running under Microsoft Windows 7. The ECD spectrum was measured on a JASCO J-1500 spectropolarimeter. Time dependent DFT simulated ECD spectra were obtained by evaluating all the possible configurations around the chiral center and their optimization in Gaussian 6 software. Then, the optimized conformers were used for ECD calculations in Gaussian 6 software using the TD-SCF DFT method and parameters B3LYP/6-31G(d,p) with the CPCM model in methanol. The calculated ECD spectra were then

compared with experimental spectra to assign the final configuration to the molecules.

3.2.2. Plant material

The bark of *Dysoxylum malabaricum* was collected from Jogs Falls, Karnataka, in May 2022 and identified by Dr. G. Ravikanth. A voucher specimen number 1131 is deposited at the herbarium of the College of Forestry, Sirsi, University of Agricultural Sciences, Dharwad, Sirsi.

3.2.3. Extraction and isolation

The shade-dried bark of *D. malabaricum* (1 kg) was crushed, coarsely powdered, and extracted three times by methanol-dichloromethane (1:1, 2L x 3) for 72 hours at room temperature. The extract was concentrated to evaporate the organic solvent, and 190 gm of crude extract was obtained. The crude extract was suspended in water and subjected to sequential fractionation using hexane and ethyl acetate. Three fractions *viz* hexane, ethyl acetate and water (250 ml each) were prepared and subjected to cytotoxicity. The cytotoxic ethyl acetate fraction was subjected to LC-MS analysis. Further active ethyl acetate fraction was loaded to silica gel column chromatography and eluted with a gradient system of ethyl acetate in n-hexane. Total 21 fractions (fr) were eluted as follows, Fr 1: 100% hexane, Fr 2: 95% hexane, Fr 3 :90% hexane, Fr 4: 85% hexane, Fr 5: 80% hexane, Fr 6: 75% hexane, Fr 7: 70% hexane, Fr 8: 65% hexane, Fr 9 :60% hexane, Fr 10: 55% hexane, Fr 11: 50% hexane, Fr 12: 45% hexane, Fr 13: 40% hexane, Fr 14: 35% hexane, Fr 15: 30% hexane, Fr 16: 25% hexane, Fr 17 : 20% hexane, Fr 18: 15% hexane, Fr 19 : 10% hexane, Fr 20: 5% hexane, Fr 21: 0% hexane. Fractions were pooled together based on their TLC profiling. A total of 6 working fractions were prepared and subjected to cytotoxicity (breast (MCF-7, T-47D, MDA-MB-232, BT549, ZR-75-30, Hs578t) lungs (A549), kidney (HEK-293) and hypopharynx cancer cell lines (FaDU) and chemo-profiling using HPLC and LCMS. Out of 6 working fractions, cytotoxic active fractions

I to IV were subjected to repeated column chromatography followed by final purification by HPLC to yield pure compounds. Compounds **1** and **2** were purified by conventional silica gel-based column chromatography from fraction I, while compounds **3**-**10** were isolated via repeated column chromatography and HPLC from fractions III to IV. The isolation of compounds **3**, **4**, and **6** from fraction II was performed using semi-preparative HPLC, where the mobile phase consisted of acetonitrile and 0.1% acetic acid in water at a flow rate of 1mL/min for a total run time of 75 min. The isocratic mode of pump flow was applied, and the HPLC-PDA detector was used to detect the individual constituents and collect the target peaks at 254 nm. Further, the collected fractions from separate runs were concentrated, dried, and characterized by spectroscopic analysis. Also, fraction III (100 mg) and fraction IV (100 mg) were subjected to analytical HPLC for the isolation of compounds **5**, **7**, **8**, **9** and **10**, where the mobile phase consisted of acetonitrile and 0.1% acetic acid in water at a flow rate of 1mL/min for a total run time of 16 min in isocratic mode of acetonitrile and 0.1% acetic acid in water (65:35) the fraction collector was adjusted to time intervals of 0-2.5, 2.6-5.0, 5.1-7.5, 5.1-7.5, 10-12.5, 12.5-15.0 min. Further, the collected fractions from the separate run were concentrated, dried, and characterized by spectroscopic analysis.

3.2.4. Cell line and cell culture

All the cell lines were obtained from NCCS Pune, India and cultured as per the protocol provided. 96-well plates and T-25 flasks were purchased from Eppendorf, DMEM (Dulbecco's Modified Eagle Medium) from Genetix (Genetix Biotech Asia Pvt. Ltd). Penicillin-streptomycin, Trypsin-EDTA, and FBS (Fetal Bovine Serum) were procured from Gibco. PBS (Phosphate Buffer Saline) was prepared using analytical chemicals.

Cells were grown in a CO_2 incubator (Esco) at 37°C with a 98% humidity and 5% CO_2 gas environment. Inhibition of cell proliferation by different compounds was measured

with the 3-(4, 5-dimethylthiazole-2-yl)-2,5-diphenyltetrazolium bromide or MTT assay. Isolated compounds were tested for cell viability against T-47D (breast carcinoma), MCF-7 (breast carcinoma), A549 (lung epithelial carcinoma), MDM-231 (breast adenocarcinoma), Hs578t (breast carcinoma), ZR-75-30 (breast carcinoma), FaDU (human pharynx squamous cell carcinoma), BT549 (breast carcinoma) and HEK-293 (Normal human kidney cells) using MTT assay. 1×10^4 cells were seeded into each well of a 96-well cell culture plate and allowed to adhere for the night. Additionally, the cells were incubated for 48 hours with varying concentrations of each compound. After removing the compound-containing medium, 100 µl of fresh MTT media were added to each well. The MTT-containing media were removed after two hours of incubation. After that, 100 µl of DMSO was added to each well and given another 30 minutes of incubation time. At 570 nm, the absorbance was determined using a multi-plate reader.

3.2.5. Apoptosis analysis by acridine orange/ethidium bromide (AO/EtBr) staining

1×10^6 number of viable cells were incubated for 3 h with increasing concentrations of compounds at 37°C separately. The cells were then washed with PBS, and 40µL of AO/EtBr solution (1 part of 100 µg/mL of AO in PBS; 1 part of 100 µg/mL of EtBr in PBS) was added just before fluorescence microscopy examination. The cells were spread on a slide and examined under a fluorescence microscope. Images were captured by a Nikon 800 fluorescence microscope at 20 and 40 times magnifications.

3.2.6. Apoptosis analysis by DAPI staining

DAPI binds to and 'stains' double-stranded DNA, preferably binding to A-T-rich regions in DNA. DAPI stain is excited by ultraviolet (UV) light, with its largest excitation wavelength at ~360nm, and it produces a vibrant blue colour with its largest emission wavelength at ~460nm when bound to DNA. Apoptosis induction was evaluated through

DAPI staining. The apoptotic bodies were significantly visible in cells treated with IC_{50} and higher concentrations of compounds for 48 h.

3.2.7. DNA content and cell cycle phase distribution

MCF-7 cells (1×10^6 cells/2 mL/well) were treated with compound at lower, IC_{50} and higher concentrations for 24 h. They were harvested and washed with 1 mL of PBS, then centrifuged at 400 rpm for 5 min at 4°C. The pellet was suspended in 100 µL of PBS and RNAase- 40 µg/mL for 90 minutes, further incubated with propidium iodide-25 µg/mL incubated at 37°C in dark for 20 min. Finally, cells were analyzed immediately on a flow cytometer FACS Calibur (Becton Dickinson, USA). The data were collected in list mode on 10,000 events and illustrated in a histogram. The number of cells (counts) was plotted against the relative fluorescence intensity of PI (FL-2; λem: 585 nm; red fluorescence). The resulting DNA distributions were analyzed by Flowjo for the proportions of cells in the G0/G1, S phase, and G2/M phases of the cell cycle.

3.2.8. Western blot analysis

Treated and untreated cells were centrifuged at 400 rpm at 4 °C, washed in PBS, and cell pellets were lysed in RIPA buffer for preparation of whole-cell lysate. An equal amount of protein (60 µg) was loaded into each well for SDS-PAGE. After setting the blots in ECL plus solution, the blots were incubated with different primary antibodies (1:1000), secondary antibodies (1:5000) and, chemiluminescence was captured on hyperfilm after incubating the blots in ECL plus solution. Antibodies Cyclin B1 4138, CDC20 4823, CDC25 4688 and SKP-2 4358, Antirabbit Secondary: 7074. were procured from cell signaling technology, USA [87].

3.3. Result and discussion

3.3.1. LC-MS-based dereplication for identification and isolation of metabolites present in the bark extract using the DNP database.

The shade-dried bark of *Dysoxylum malabaricum* was powdered and extracted three times using methanol-dichloromethane (1:1) at room temperature. The crude extract obtained after filtration and solvent evaporation under reduced pressure was suspended in distilled water and fractionated sequentially with hexane and ethyl acetate, as described in Figure 3.2.

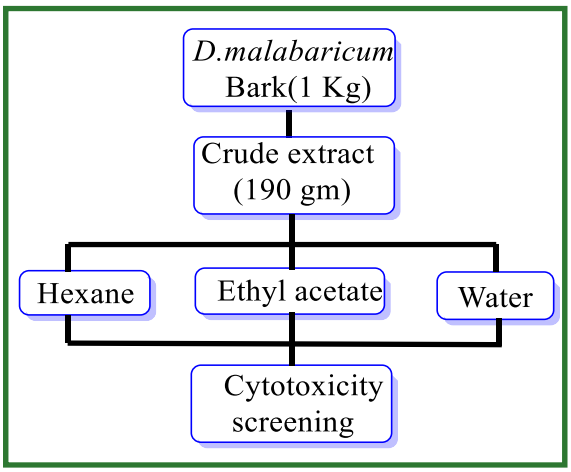

Figure 3.2. Schematic diagram of extraction of *D. malabaricum* bark.

All three fractions, *viz* hexane, ethyl acetate and water were concentrated and subjected to cytotoxicity screening against MCF-7, A549, MDAMB-231, Hs578t, ZR-75-30, FaDU, T-47D and BT-549 cancer cell lines. Of all the fractions, the ethyl acetate fraction displayed the most pronounced cytotoxicity against breast cancer cell line exhibiting IC_{50} in the range of 15-85 µg/mL (Table 3.1).

Table 3.1. MTT assay of ethylacetate fraction after 48 hours.

	MTT Assay (IC_{50} in µg/mL)							
Fractions	A-549	MCF-7	T-47D	MDA-MB-231	BT-549	ZR-75-30	FaDU	Hs578t
Ethyl acetate	87±1.13	25±1.76	20±2.10	36±1.61	42±2.05	74±1.28	89±1.48	83±2.81

This fraction was subjected to bioassay-guided fractionation through silica gel column chromatography using hexane and ethyl acetate as mobile phase in a step gradient manner (increasing the concentration of ethyl acetate by 5% starting from 100% hexane to 100% ethyl acetate). Twenty-one fractions, each 200 ml volume, were collected and pooled into six fractions based on the TLC profiling. The cytotoxicity of these six fractions was then evaluated against a panel of cancer cell lines, as mentioned before, and four fractions showed more than 50% growth inhibition of breast cancer cells. The active fractions were further profiled using liquid chromatography. The UV and mass spectra were recorded using HPLC with a photodiode array detector (PDA) and LC-MS analysis, respectively. The general workflow of isolation is represented in Figure 3.3.

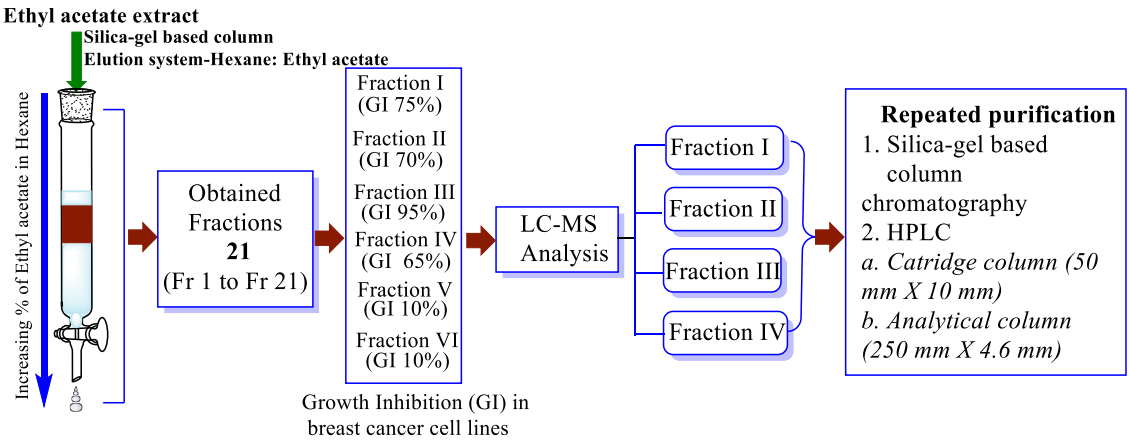

Figure 3.3. Workflow of bioassay-guided fractionation and isolation.

3.3.1.1. LC-MS analysis of bark extract

In this study, a dereplication strategy was applied to identify cytotoxic compounds from the active ethyl acetate fraction rapidly. During the analysis of LC-MS spectra, multiple peaks in the *m/z* 400 to 600 range were observed, eluting from 13 to 25 minutes. All the observed peaks exhibited similar UV spectra in the range of 190 to 220 nm, suggesting that the compounds might belong to the same class, having a mass range of 400-600 and limited visibility under UV light. In the visual examination of the total ion chromatogram (Figure 3.4) the predominantly ionized components were observed to be *m/z* 415.2116,

455.3541, 469.3319, 471.3462, 473.3621, 485.3254, 487.3412 491.3611, 503.3362, 511.3389, 513.3550, 517.3523, 519.3901 and 523.3420 in ESI-positive mode listed in Table 3.2. MS/MS fragments revealed various common daughter ions such as *m/z* 105, 121, 127, 123, 143, 173, 175, 203, 207, 219, 221, 235, and 249. From the observed fragmentation patterns, it was inferred that all the compounds likely belong to the same class, concluding the presence of triterpenoids. To optimize the dereplication process for novel compound identification, the DNP database was utilized, and the preliminary data obtained from mass spectrometry analysis was strategically harnessed.

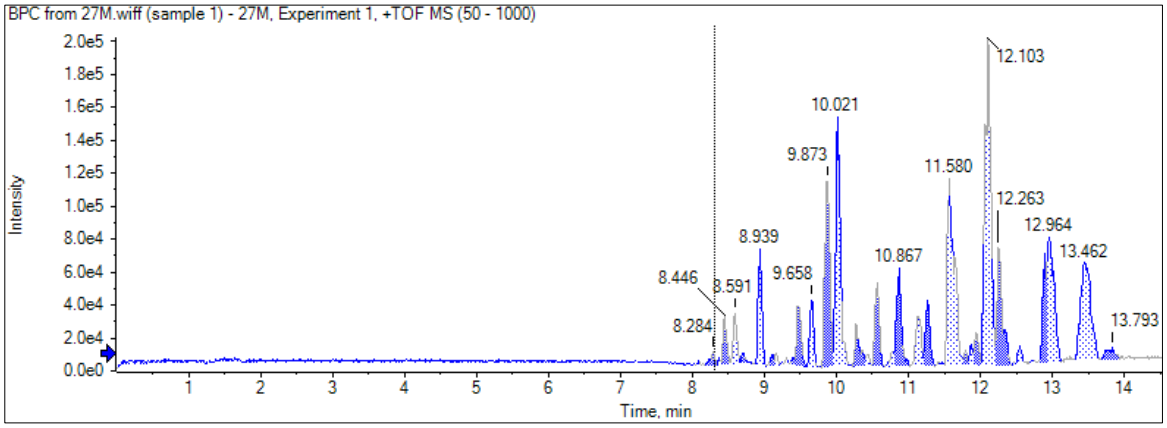

Figure 3.4. LC-MS profiling of ethyl acetate active fraction.

Table 3.2. List of detected molecular ion peaks for dereplication.

t_R (min)	Mass (Observed)	Cald (ppm error)	MF [c]	Inference
9.48	491.3611 $(M+H)^+$ 513.3550 $(M+Na)^+$ 529.3210$(M+K)^+$	491.3731(2.40)	$C_{30}H_{50}O_5+H^+$	New metabolite
9.67	489.3502 $[M+H]^+$ 511.3378$[M+Na]^+$	489.3513(2.25)	$C_{30}H_{48}O_5+H^+$	New metabolite
9.88	503.3362 $(M+H)^+$ 525.3177 $(M+Na)^+$ 543.3652$(M+ACN)^+$	503.3367 (0.99)	$C_{30}H_{46}O_6+H^+$	New metabolite
10.04	415.2116 $(M+H)^+$ 437.194 $(M+Na)^+$	415.2115 (0.24)	$C_{24}H_{30}O_6+H^+$	New metabolite[b]
11.11	471.3470 (M+H)+ 493.3276 (M+Na)+ 511.3545$(M+ACN)^+$	471.3464 (1.27)	$C_{30}H_{46}O_4+H^+$	New metabolite (Fraction II)
11.29	471.3462 $(M+H)^+$ 511.3389$(M+ACN)^+$ 512.3423$(M+ACN+H)^+$	471.3464 (0.42)	$C_{30}H_{46}O_4+H^+$	New metabolite
11.55	473.3621 $[M+H]^+$ 513.3532 $(M+Na)^+$	473.3631 (-2.11)	$C_{30}H_{48}O_4+H^+$	New metabolite
12.09	469.3319 $(M+H)^+$ 491.3141 $(M+Na)^+$	469.3316 (0.59)	$C_{30}H_{44}O_4+H^+$	Binecterilactone (**2**)[d]
12.96	485.3254 $(M+H)^+$ 507.3074 $(M+Na)^+$ 991.6226 $(2M+Na)^+$	485.3262 (-1.64)	$C_{30}H_{44}O_5+H^+$	Beddomeilactone (**1**)[a]
13.07	487.3412 $(M+H)^+$ 509.323 $(M+Na)^+$ 995. 6559 $(2M+Na)^+$	487.3418 (-1.23)	$C_{30}H_{46}O_5+H^+$	New metabolite

[a]DNP results based on the input as follows; *biological source*: *Dysoxylum*, *molecular formula by elements*: C 30, and *substructure search*: fused cyclopropane ring. [b]Minor observed in LC-HRMS and assumed to be new based on dereplication, couldn't be purified sufficient to characterize fully. [c] Molecular formula (MF), [d] Reported in January 2023.

3.3.1.2. DNP-based dereplication using LC-MS data

The dictionary of natural products database was selected for establishing a dereplication strategy containing various properties as input for the search queries (Figure 3.5). Using the *'biological source'* property as a search query in the DNP database, 380 hits related to the genus *Dysoxylum* were obtained. To narrow the results further, we refined our search by selecting 'types of compounds' such as triterpenoid, which yielded 184 hits (Figure A.1 in appendix). The DNP search was further refined using parameters such as 'accurate mass ranges' and 'elements' to advance the dereplication process for each targeted mass ion peak revealed in LC-MS analysis. These search queries were used to dereplicate the

spectral information, resulting in the identification of known or new compounds before the isolation process. Further, characteristic peaks obtained from the 1D NMR experiment were introduced into the DNP database with the additional search query "structure fragment," which added an advantage in determining the basic skeleton present in the isolated compounds. According to the DNP database, only six triterpenoids have been isolated from *Dysoxylum malabaricum* (Figure A.2 in appendix). Therefore, the DNP-based dereplication strategy concluded that various molecular ion peaks observed in LC-MS spectra reveal the presence of new metabolites of the same class of triterpenoids present in *D.malabaricum* bark extract.

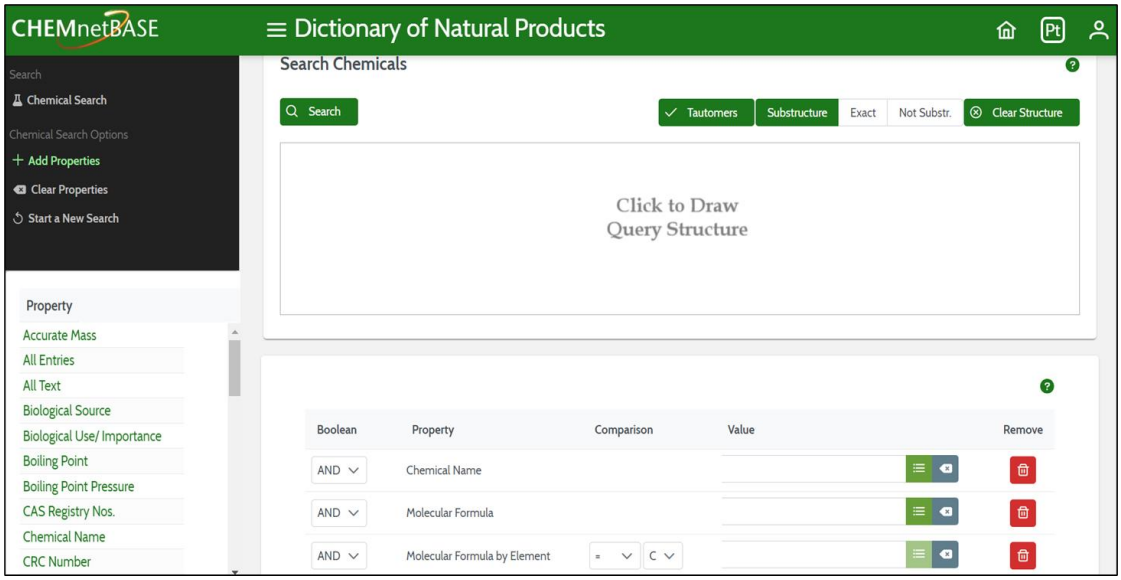

Figure 3.5. Dictionary of Natural Product Database.

3.3.2. Structure elucidation and cytotoxicity screening of compounds isolated from fractions I and II.

3.3.2.1. Structure elucidation of compounds targeted and isolated fractions I and II

During the phytochemical investigation of ethyl acetate active fractions I and II, the five most abundant peaks were targeted, which were observed in LC-MS spectra, and the obtained information was dereplicated using the DNP database to find out the novelty of the structure. These compounds were isolated, purified, and characterized using extensive

spectral analysis. The most abundant mass peak that appeared prominently in fraction 1 at *m/z* $[M+H]^+$ 485.3255 was deduced to the molecular formula $C_{30}H_{44}O_5+H^+$. The data was methodically processed into the DNP for dereplication, and this search, based on the accurate mass range of 484.000 to 484.999, yielded seven hits. An additional search parameter specifying '*elements*' with correspondence to C30 was incorporated, narrowing the results to just three hits. The target compound was assumed to be among the hit list items or represent a novel triterpenoid (Appendix Figure A.3). Thus, it was isolated via silica gel-based column chromatography. After the purification of compound **1,** the ^1H NMR analysis revealed two protons doublet at δ_H 0.72 and δ_H 0.79 coupled to each other in the up-field region, confirming the presence of a fused cyclopropane ring. Consequently, based on this evidence, we excluded the potential of different compounds and determined that beddomeilactone [88], which possesses the fused cyclopropane ring, was the likely candidate (Figure 3.6). Further detailed characterization using 2D NMR, combined with ECD and TD-DFT-simulated ECD spectrum, as shown in Figure A.6-A.11 in the appendix, confirms the stereochemistry of compound **1**, and it was identified as a ring-modified cycloartane type of triterpenoid, beddomeilactone.

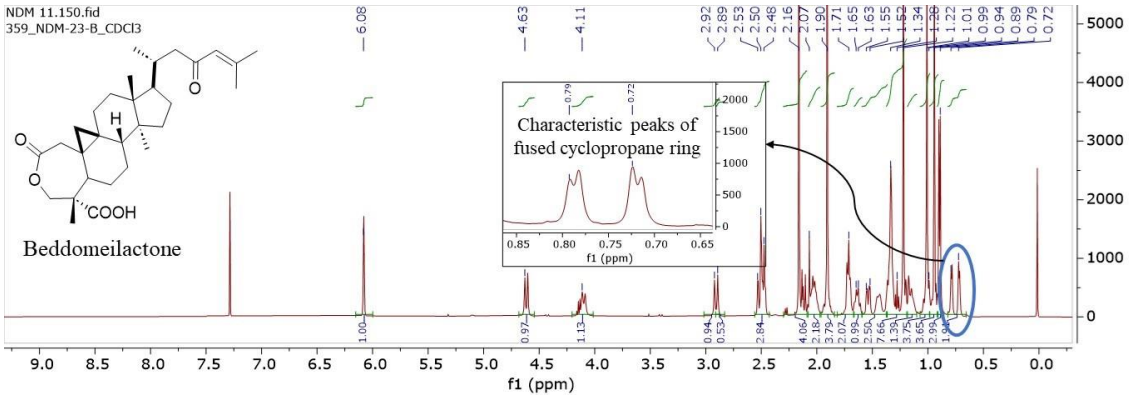

Figure 3.6.^1H NMR of beddomeilactone (**1**)

The LCMS profile of fraction 1 showed the second most abundant ion peak at *m/z* 487.3412 $[M+H]^+$, which is 2.0158 Da more than the beddomeilialactone. The spectral information was dereplicated and introduced in the DNP database which resulted in zero

hits. Compound **2** was assumed as a dihydro derivative of beddomeilialactone with saturated ketone-containing side chains. Additional CH_2 observed at C24 (52.4 ppm) was confirmed by DEPT-135 (Figure 3.7) and showed COSY with a proton at δ_H 1.10 ppm (C25). Further, the protons attached to three different carbon atoms, C25(δH 1.10 ppm), C26 (δH 0.68 ppm), and C27 (δH 0.68 ppm) showed HMBC correlation with the methylene carbon present at C24, depicting compound 2 as a new metabolite, characterized as dihydrobeddomeilactone (Figure 3.8).

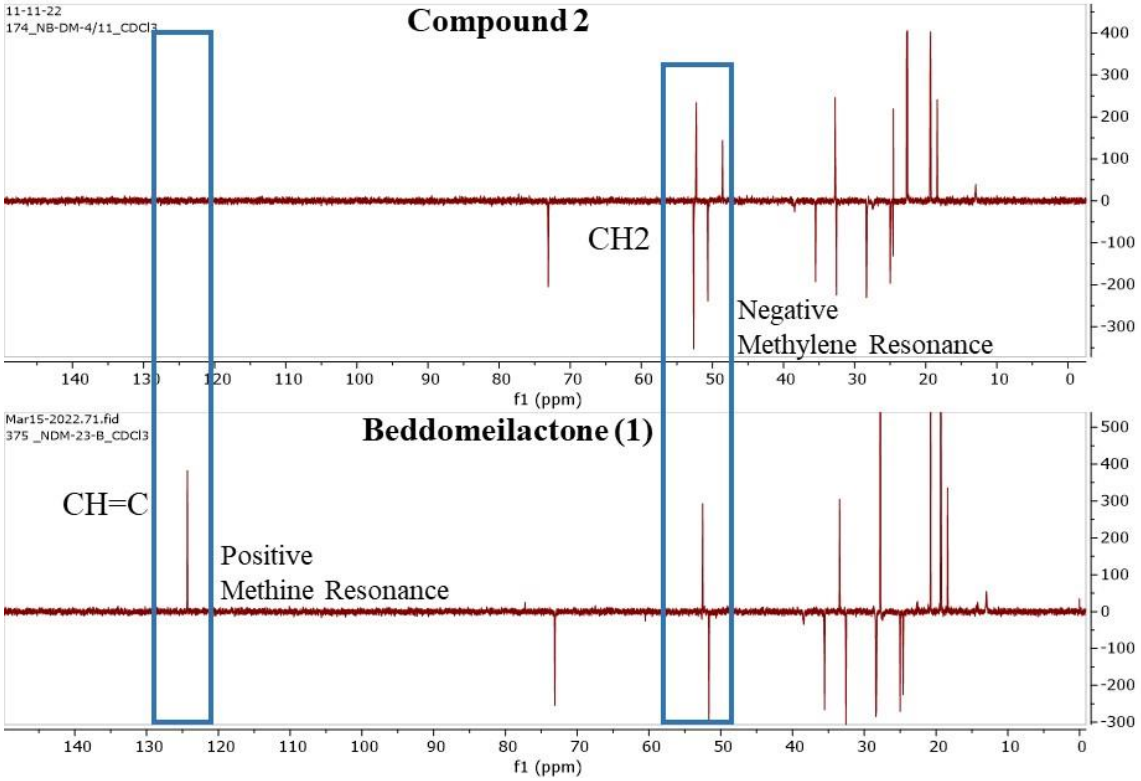

Figure 3.7. Comparative study of DEPT-135 spectra of compounds **2** and **1**.

The relative stereochemistry of compound **2** was established by NOESY correlations and by performing ECD, and time-dependent DFT simulated ECD experiments (Figure 3.9). Dihydrobeddomeilactone was characterized as (1S,5aS,6aS,8aR,9R,11aS,11bS)-1,8a,11a-trimethyl-9-(6-methyl-4-oxoheptan-2-yl)-4-oxotetradecahydro-2H,6H-cyclopenta[5,6] cyclopropa[1,8a]naphtho[1,2-d]oxepine-1-carboxylic acid. (Appendix Figure A.12-A.16).

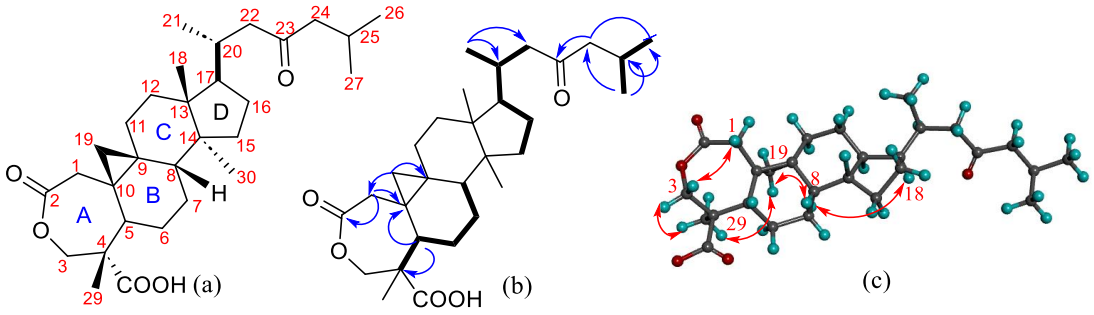

Figure 3.8. a) Structure (b) Major HMBC ( ), COSY ( ) and (c) NOESY( ) correlations of compound **2**.

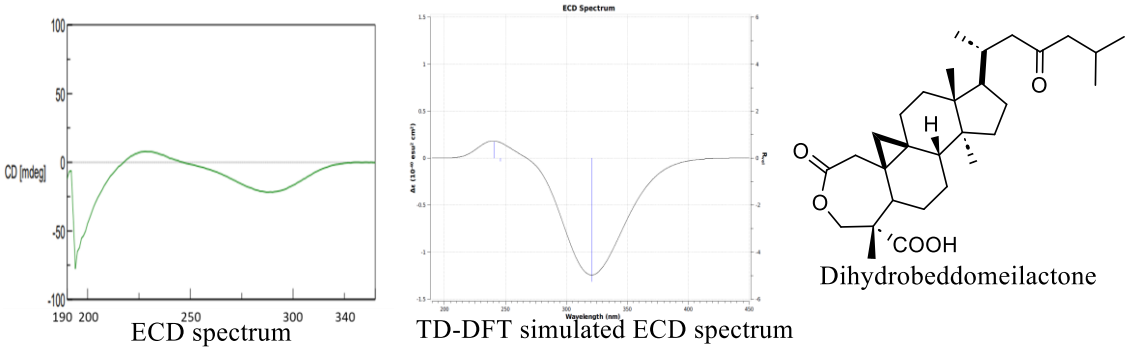

Figure 3.9. Stereochemistry of dihydrobeddomeilactone (**2**).

Furthermore, the mass ion peak obtained at *m/z* 503.3569 was targeted in fraction II, which corresponds to the molecular formula $C_{30}H_{46}O_6+H^+$. The DNP-based dereplication search resulted in the four hits. Results were later refined after recording ^{1}H NMR, confirming the presence of the cyclopropane ring and corresponding protons appearing in the upfield region of ^{1}H NMR (< δ_H 0.72 ppm). DNP search resulted in a single hit corresponding to a cycloartane compound with a molecular formula having 32 carbon atoms in the structure. The possibility of this compound was dismissed because compound **3** exhibited a molecular formula consistent with C30. This compound was assumed to be new as the molecular formula of the reported compounds was different (Appendix Figure A.4). It was purified as a white powder. Based on positive HRMS data, sodium ion adduct $[M+Na]^+$ was observed at *m/z* 525.3169, which was 16 Da more than the dihydrobeddomeilactone (**2**). Comparison of its NMR data with those of compound **2** revealed similar features in rings A−D. It was assumed to be a hydroxy derivative of

compound **2** with an additional OH group. 2D NMR was recorded for the complete structural characterization of this compound. ^{13}C NMR confirmed the absence of any double bond and corresponding additional CH_2 observed in the DEPT-135 at 54.4 ppm (C24) at the terminal methyl group attached to the aliphatic side chain (Figure 3.10).s

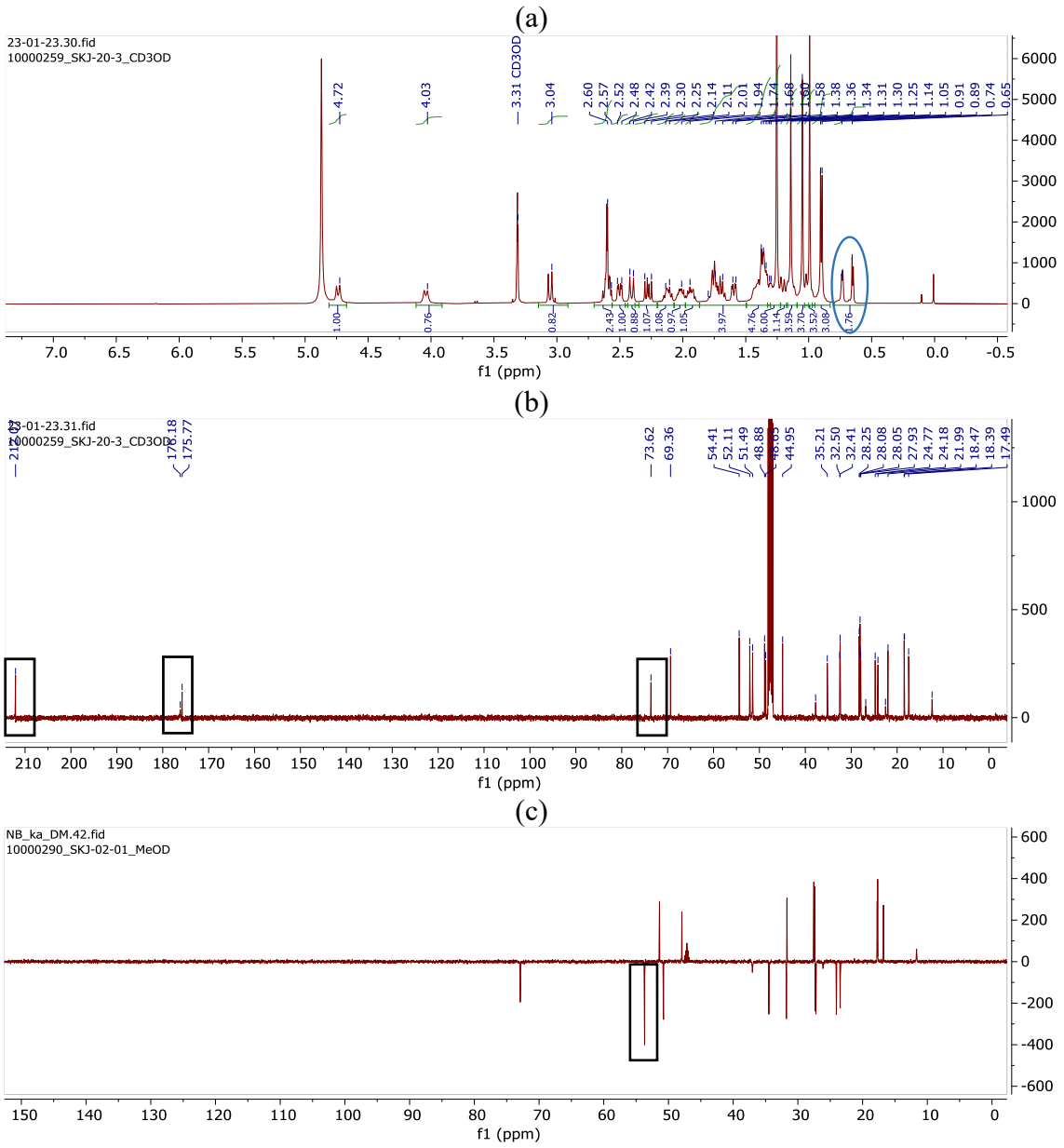

Figure 3.10. (a) ^{1}H NMR (b) ^{13}C NMR (c) DEPT-135 NMR spectra of compound **3**.

Moreover, HMBC confirmed the correlation between C24 and proton attached to C26 (δ_C 28.1 ppm, δ_H 1.05 ppm) and C27 (δ_C 28.2 ppm, δ_H 1.25 ppm); both methyl proton at C26 (δ_H 1.25 ppm) and C27 (δ_H 1.25ppm) showed HMBC correlation to quaternary carbon at

C25 (δ_C 69.4) as shown in Figure 3.11. NOESY data determined the relative configuration of compound **3** (Appendix Figure A.17-A.19). To fix the spatial arrangement of atoms, the relative configuration of compound **3** was determined by ECD experiment and was compared with the TD-DFT-simulated ECD spectrum shown in Figure 3.12.

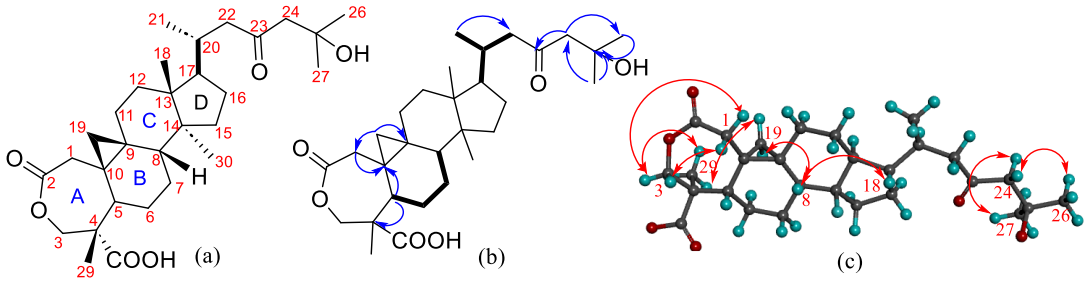

Figure 3.11. a) Structure (b) Major HMBC ( ), COSY ( ) and (c) NOESY( ) correlations of compound **3**.

Finally, it was characterized as (1S,5aS,6aS,8aR,9R,11aS,11bS)-9-(6-hydroxy-6-methyl-4-oxoheptan-2-yl)-1,8a,11a-trimethyl-4-oxotetradecahydro-2H,6H-cyclopenta[5,6] cyclopropa[1,8a]naphtho[1,2-d]oxepine-1-carboxylic acid and named as hydroxy derivative of beddomeiliactone (**3**).

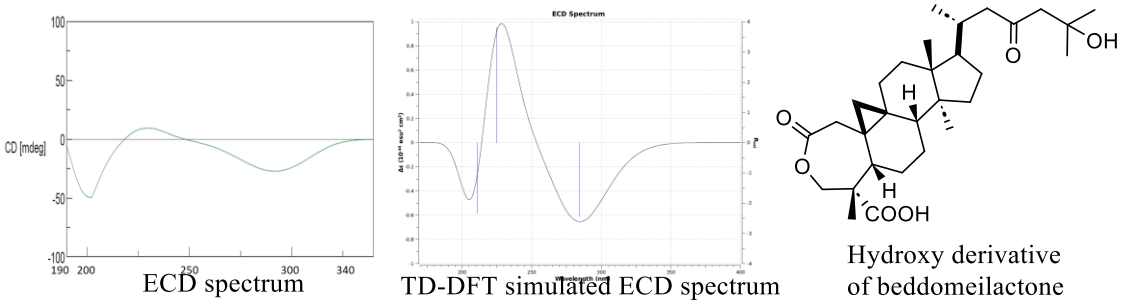

Figure 3.12. Stereochemistry of hydroxy derivative of beddomeilactone (**3**).

Next, compound **4** was isolated, which showed mass peak *m/z* at 471.3487 for molecular formula $C_{30}H_{46}O_4$+H^+ and its acetonitrile adduct $[M+CH_3CN]^+$ at *m/z* 511.3378 in HRMS spectra. Generally, chemical structures containing simple alcohol in their basic skeleton show acetonitrile adduct, as it is the most common solvent used in LC-MS quantification [89]. The obtained structural features were introduced to the DNP database as search

query properties resulted in 17 hits; further, the result was narrowed to 14 hits by the addition of the search query 'molecular formula' corresponding to C30. The HPLC purification followed by ^{1}H NMR found several spectral properties identical to compounds **1**-**3,** demonstrating the presence of a fused cyclopropane ring. Consequently, it was assumed to be a cycloartane triterpenoid; hence, the 'substructure search' query was applied in DNP, which resulted in two hits. But these two hits had the additional cyclic ring in place of the aliphatic side chain. This confirmed that the isolated compound could be a new cycloartane triterpenoid and, therefore, subjected to detailed spectral characterization. The DNP search further for *D. malabaricum* resulted in zero hits, indicating compound **4** as a new metabolite (Appendix Figure A.5). The 1D and 2D NMR data of compound **4** suggested the existence of the same carbon skeleton as compounds **1**-**3**, except for differences in ring A. Fortyfour proton resonance was observed in ^{1}H NMR spectrum (Figure 3.13 a). Two carbonyl and ten methylene groups were noticed from the ^{13}C NMR and DEPT-135 spectra (Figure 3.13 b and c). The presence of CH_2OH and the absence of the carboxylic group were observed at the 4a position of ring A. Only one carboxylic carbon and eleven methylene groups were observed in ^{13}C and DEPT-135 NMR spectra, respectively (Appendix Figure A.23). This infers the presence of CH_2OH instead of COOH in compound **4**.

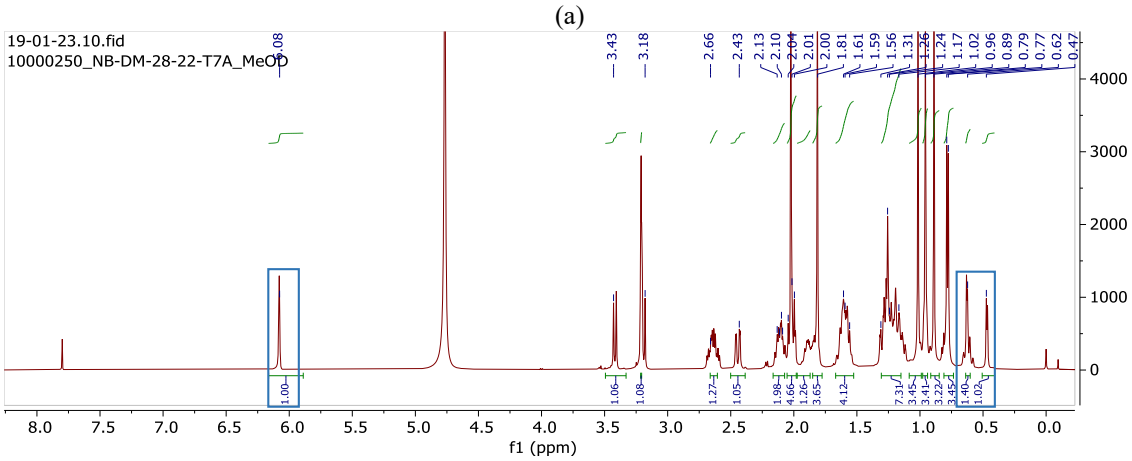

Figure 3.13. (a) ^{1}H NMR spectrum of compound **4**.

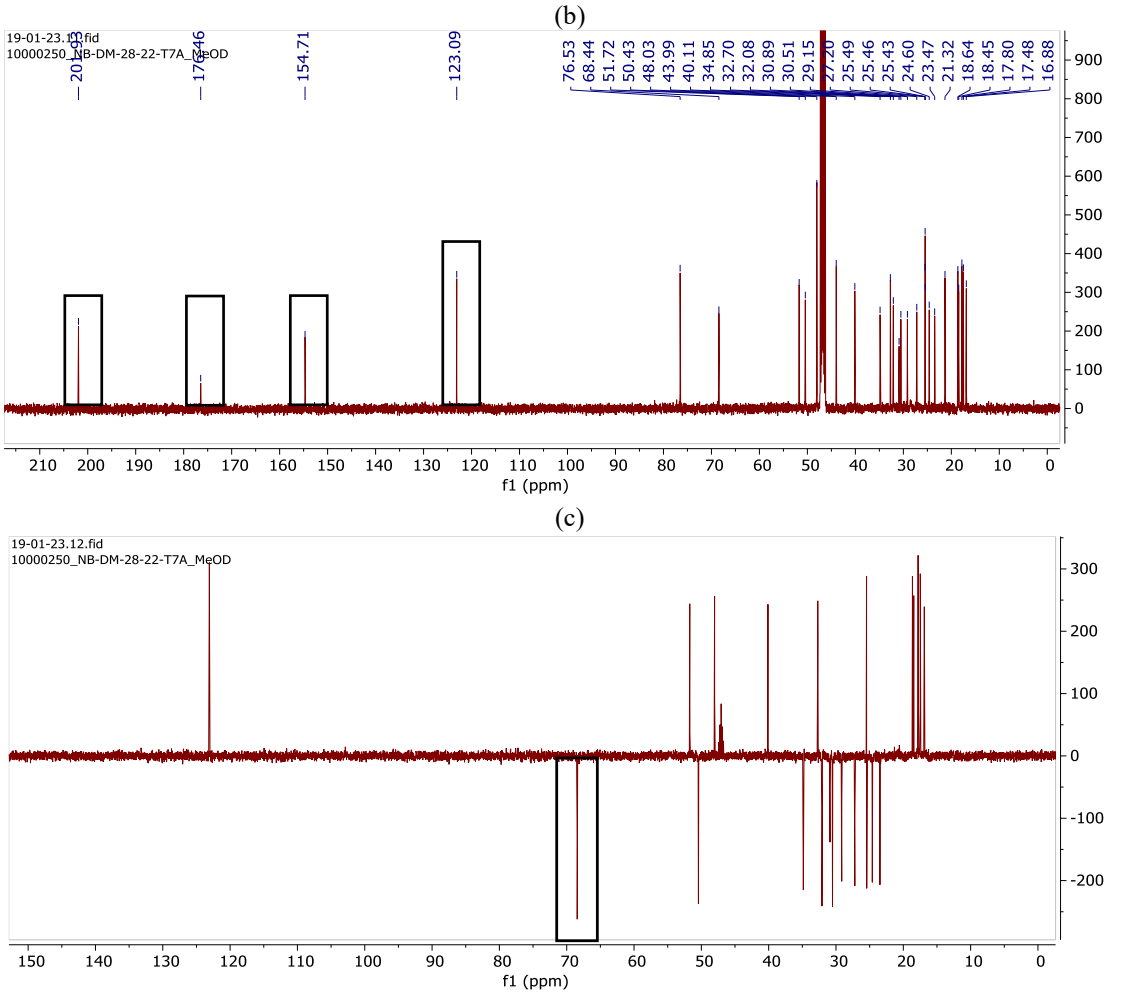

Figure 3.13. (b) ^{13}C NMR and (c) DEPT-135 spectra of compound **4**.

The methyl proton at δ_H 0.96 showed four significant HMBC correlations with carbon at δ_C 16.8 (CH_3), δ_C 40.1 (CH), δ_C 68.4 (CH_2OH), and δ_C 76.5 (C). The proton of CH (δ_C 40.1) at δ_H 2.00 showed correlations with cyclopropane ring's CH_2 (δ_H 2.66 and δ_H 1.21)

and quaternary carbon at δ_C 24.6 and δ_C 76.5. The junction quaternary carbon at δ_C 24.6 correlated with protons at δ_H 2.66 and δ_H 1.21 attached to C-1 (δ_C 30.5) and CH_2 of cyclopropane ring proton at δ_H 0.62 and δ_H 0.47 attached to carbon at δ_C 29.2 (Figure 3.14 a and c).

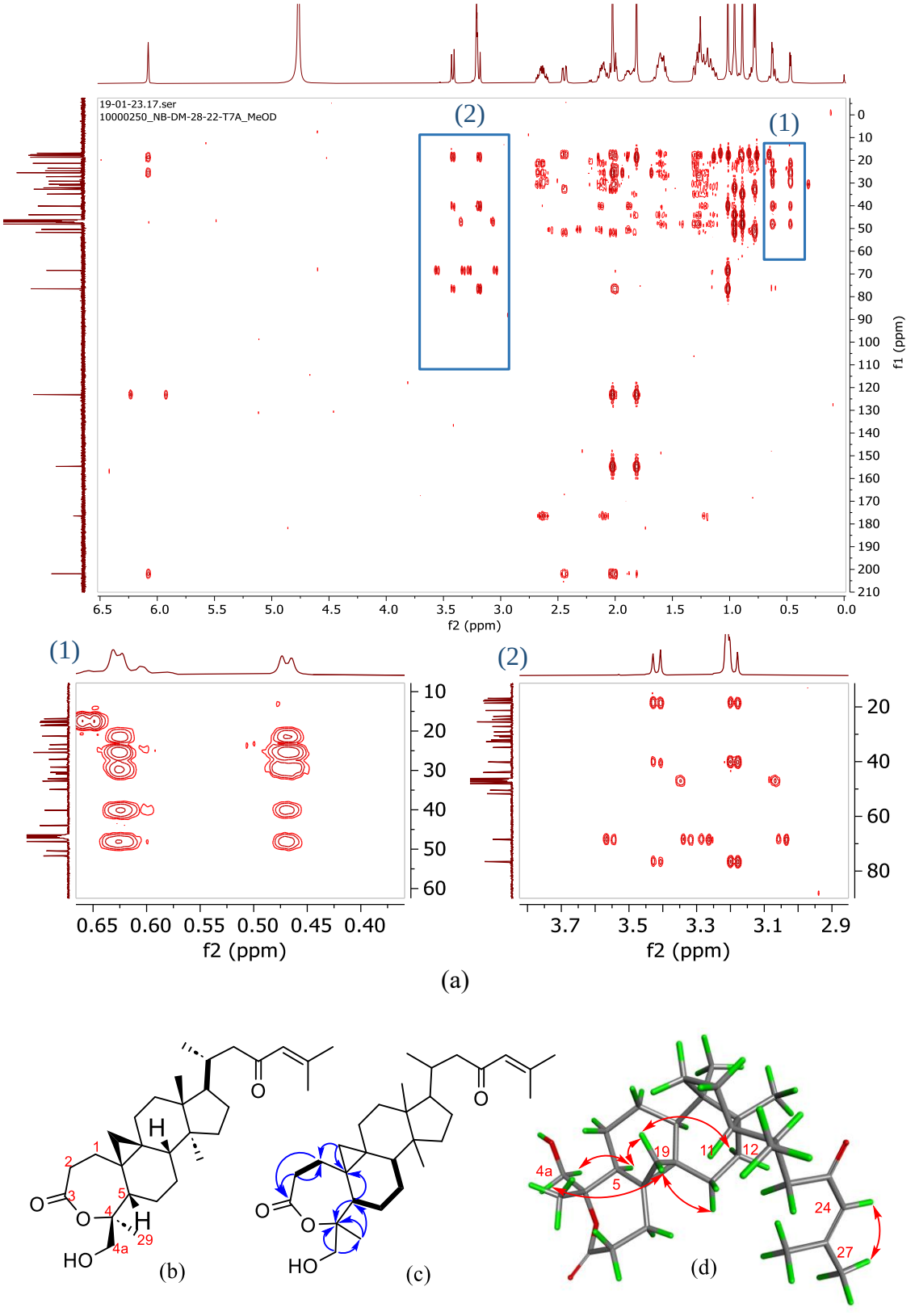

Figure 3.14. (a) HMBC spectra (b) Structure (c) Major HMBC( ) COSY ( ), and (d) NOESY ( ) correlations of compound **4**.

From the COSY data, a spin system was observed among the methylene protons of the cyclopropane ring at δ_H 0.62 and δ_H 0.47. The coupling of protons of C-1 (δ_H 2.66 and δ_H 1.26) and C2 (δ_H 2.09) was also noticed. The protons of the ring B carbon C-5 (CH, δ_H 2.00), C-6 (CH_2, δ_H 2.11 and δ_H 1.88), C-7 (CH_2, δ_H 1.24), and C-8 (CH, δ_H 1.31) were fixed by COSY correlations. The structural feature of ring A of compound **4** is fused ϵ-caprolactone fused at 4 and 5 positions. In comparison, in beddomeilactone the ϵ-caprolactone was fused at 3 and 4 positions as shown in Figure 3.15. The stereochemistry of ring A was determined by analyzing the cross-peaks, while no cross-peaks were observed between H-4a/H-29 in the NOESY spectrum, suggesting their spatial arrangement in different planes. However, H-4a/H-29, H-4a/H-5, and H-5/H-19 showed NOE coupling (Appendix Figure A.20-A.22). Compound **4** showed a negative cotton effect as optical rotation decreases on decreasing wavelength, and geometric maximum (peak) and minimum (troughs) were observed in the ECD spectra in Figure 3.16. The experimental and TD-DFT-simulated ECD spectra showed a good match and unveiled the stereochemistry of compound **4** and characterized it as (1S,5aR,6aS,8aR,9R,11aS,11bS,13aS)-1-(hydroxymethyl)-1,8a,11a-trimethyl-9-(6-methyl-4-oxohept-5-en-2-yl)tetradecahydro-3H,6H-cyclopenta[5,6]cyclopropa [1,8a]naphtho[2,1-c]oxepin-3-one and named as mahamanalactone A [90].

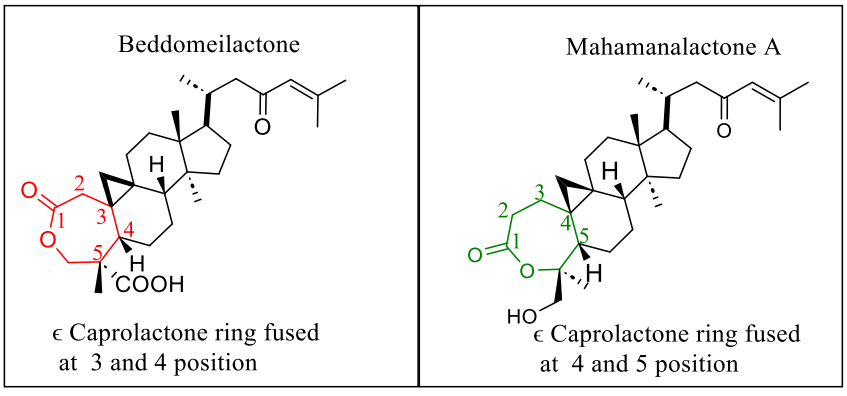

Figure 3.15. Structural feature of ring A present in beddomeilactone and mahamanalactone A.

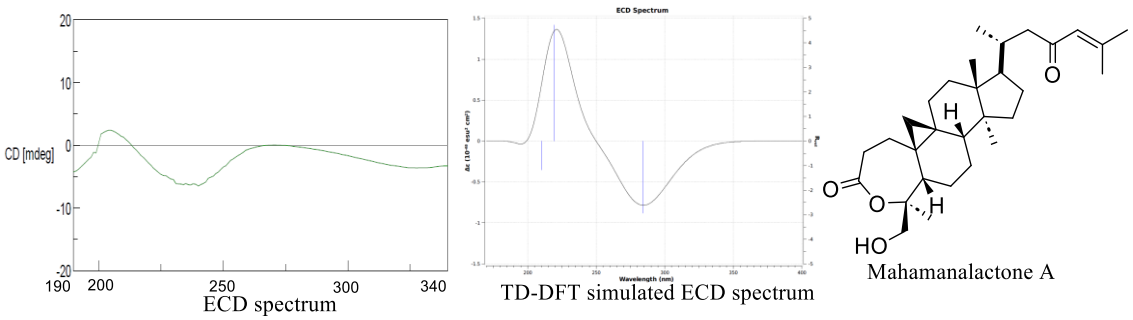

Figure 3.16. Stereochemistry of mahamanalactone A (**4**).

Further, using analytical HPLC a mass peak at *m/z* 473.3621 was isolated at the time interval of 11.57-12.05 min. The deduced molecular formula for this isolated compound **5** was found to be $C_{30}H_{48}O_4$+H^+ and its acetonitrile adduct $[M+CH_3CN]^+$ at *m/z* 513.3532 was observed in HRMS spectra. Compound **5** showed several spectral properties identical to compounds **1**-**4** and also possess a fused cyclopropane ring. The dereplication of spectral information using DNP database suggested this compound to be again new with cycloartane triterpenoid skeleton system. Also, this compound showed a 2 Da difference in molecular weight as compared to previously isolated compound **4**. Two carbonyl and ten methylene groups were noticed from the ^{1}H NMR ^{13}C NMR and DEPT-135 spectra. The methyl proton at δ_H 0.86 ppm showed four significant HMBC correlations with C at δ_C 48.1 ppm (CH), δ_C 67.5 ppm (CH_2OH), and δ_C 77.1 ppm (C).

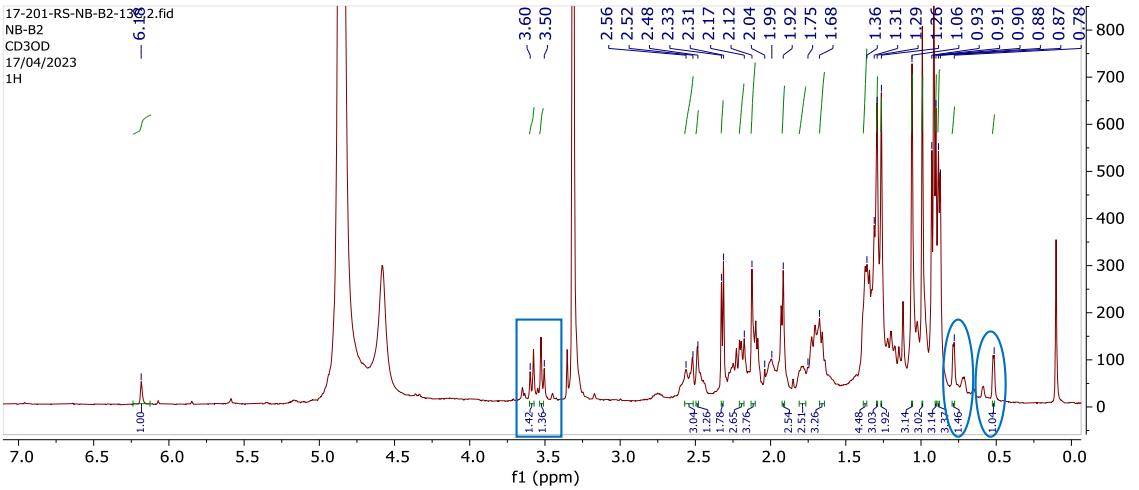

Figure 3.17. (a) ^{1}H NMR spectrum of compound **5**.

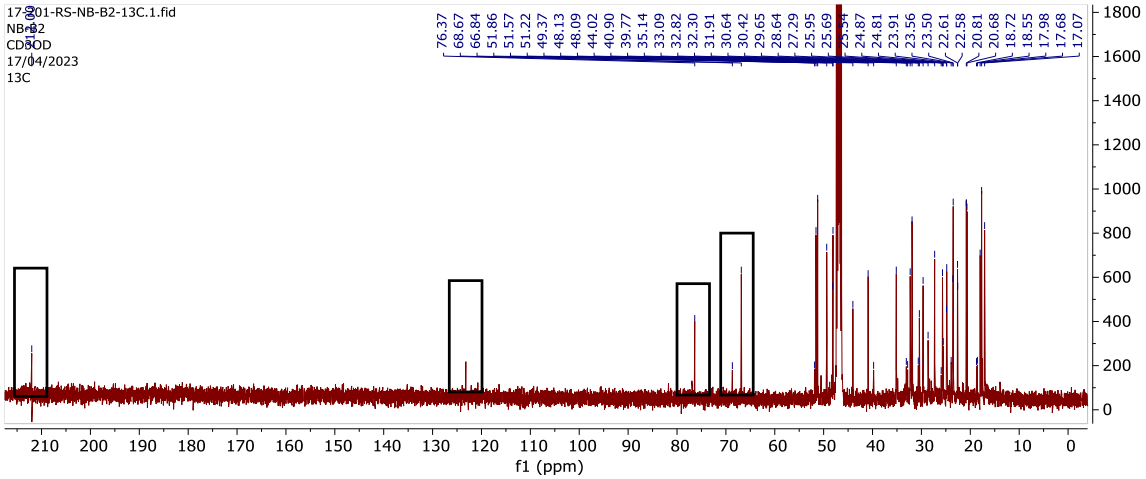

Figure 3.17. (b) ^{13}C NMR spectrum of compound **5**.

The proton at δ_H 1.31 ppm attached to C5 (δ_C 48.1 ppm) showed three significant HMBC correlations with CH2 (C19, 29.7 ppm) of cyclopropane ring and quaternary carbon at C9 (δ_C 21.1 ppm) and C10 (δ_C 20.7 ppm). The spectral analysis suggested a similarity in the chemical structure of compounds **4** and **5** (Figure 3.17 and 3.18). All structural features were similar except for the absence of one double bond at the aliphatic side chain adjacent to a carbonyl group that concluded the structure as a dihydro derivative of compound **4**. The spectra from experimental ECD and TD-DFT-simulated ECD (Appendix Figure A.26) unveiled the relative configuration of compound **5** and it was named dihydromahamanalactone A.

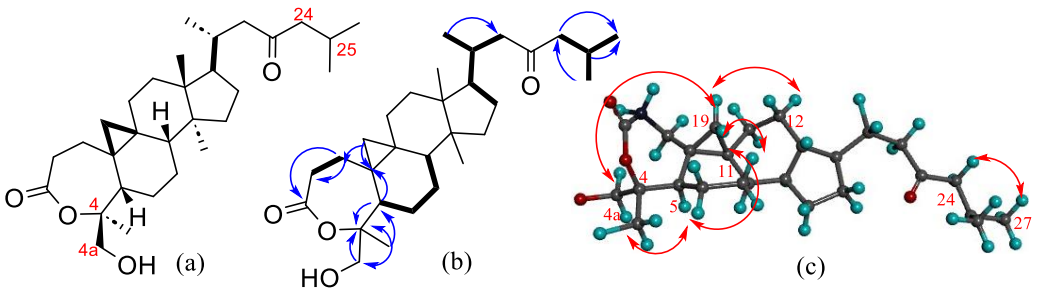

Figure 3.18. (a) Structure (b) Major HMBC ( ), COSY( ) and (c) NOESY ( ) of compound **5**.

3.3.2.2. Cytotoxicity screening of isolated compounds from fractions I and II

The ethyl acetate fraction of bark extract of *D.malabricum* was highly active against breast cancer cell lines. Therefore, to evaluate the cytotoxicity potential of the isolated compounds beddomeilactone (**1**), dihydrobeddomeilactone (**2**), Hydroxy derivative of beddomeilactone (**3**), dihydromahamanalactone A (**5**) obtained from fractions I to II were screened against breast cancer cell lines using MTT assay. These isolated compounds from fractions I and II were evaluated against T-47D, MDA-MB-231, MCF-7 breast cancer cells and HEK-293 normal human embryonic kidney cell lines. The findings showed that significant cytotoxicity was detected in a concentration-dependent manner (Figure 3.19 A). The percent viability of breast cancer cells decreased as the concentration of the compounds was increased as displayed in Figure 3.19 A. In case of T-47D and MCF-7 breast cancer cell lines, the IC_{50} values of **1-3** were determined in the range of 18-80 µM, while **5** showed no appreciable cytotoxicity. Compound **2** showed the highest cytotoxicity with IC_{50} 18 µM, 22 µM, and 40 µM against T-47D, MCF-7 and MDA-MB-231 cell lines, respectively. The IC_{50} calculated for **1** against the breast cancer cell line was 20-60 µM. While **3** showed moderate cytotoxicity, having IC_{50} 30-40 µM against T-47D, MCF-7, and MDA-MB-231 breast cancer cell lines. All the compounds did not display any substantial cytotoxicity in normal HEK-293 cells.

3.3.2.3. Apoptotic cell death induced by dihydrobeddomeilactone (2)

Dihydrobeddomeilactone exhibited the highest level of cytotoxic effect against T-47D cells. Further investigation was conducted to determine whether the cytotoxicity was attributed to apoptotic cell death. To validate the apoptotic pathway of cell death induced by dihydrobeddomeilactone in breast cancer cells, a fluorescent microscopy study was done to observe the changes in cell morphology and mode of cell death by acridine orange and ethidium bromide staining. As observed from Figure 3.19 B, the cells treated with

dihydrobeddomeilactone at a concentration of 18 µM showed altered nuclear morphology, chromatin condensation, and loss of cytoplasm. The control group containing T-47D cells showed green fluorescence with normal cell morphology with intact nuclei. However, at a lower concentration, the treated cells showed yellowish-green fluorescence depicting early apoptosis. While at higher concentrations, orange-red fluorescence was observed, representing late apoptosis in cancer cells. Additionally, at 18 µM concentration, both early and late apoptosis [91].

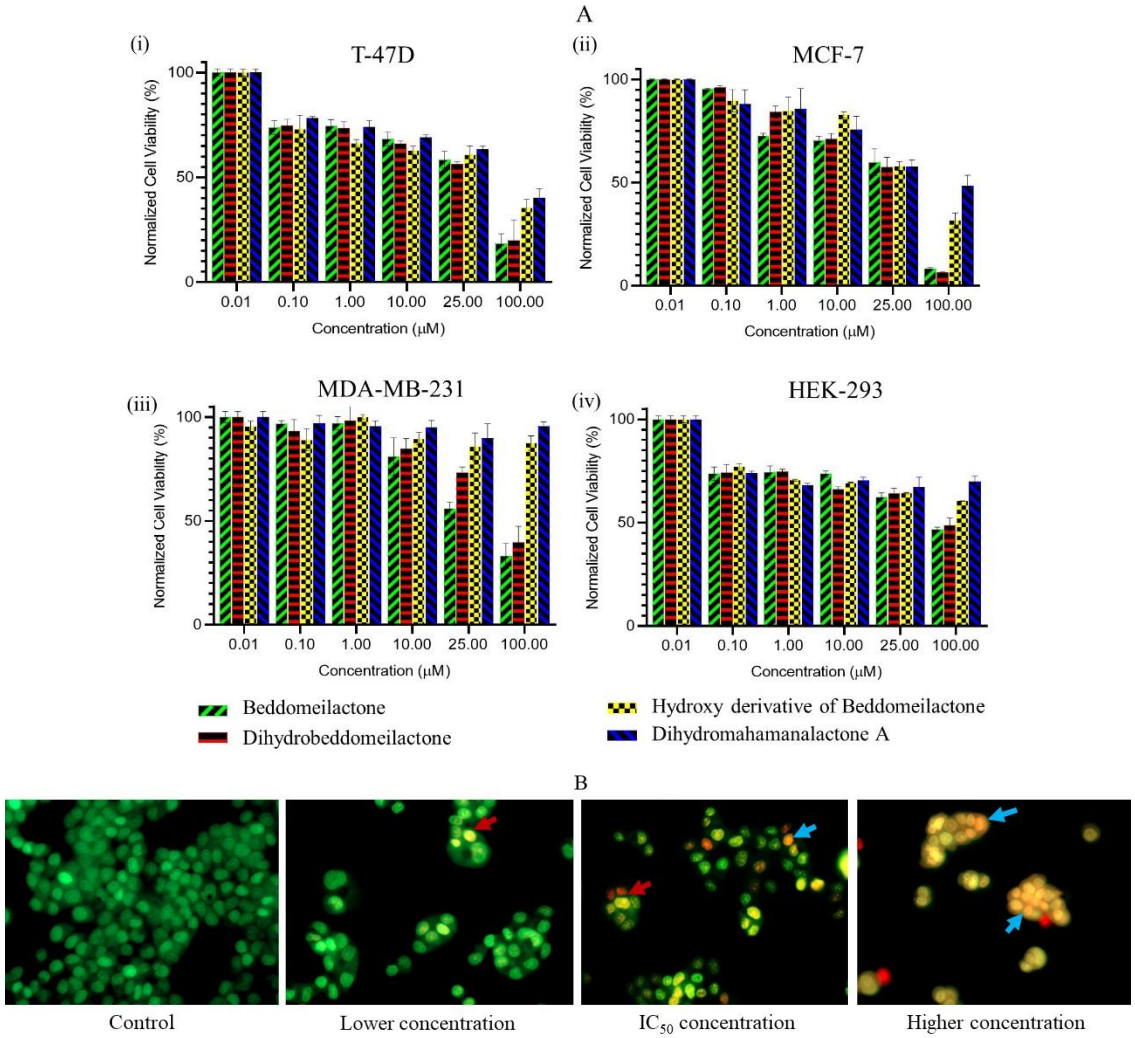

Figure 3.19. A) Normalized cell viability of (i) T-47D, (ii) MCF-7, (iii) MDA-MB-231, (iv) HEK-293 cells after 48 h treatment with compounds (Concentration µM). (B) Acridine orange-based cellular staining of treated T-47D cells where the effect of dihydrobeddomeilactone on cellular and nuclear morphology was observed. At 10 µM, early apoptosis was noticed (red arrow), and late apoptosis was observed at 100 µM (blue arrow).

3.3.3. Structure elucidation and cytotoxicity screening of compounds from fraction III

3.3.3.1. Structure elucidation of compounds targeted and isolated from fraction III

Using the established methodology of the previous section, three new mass peaks were targeted from LC-MS spectra of fraction III. Further, these targeted metabolites were isolated, purified by repeated column chromatography and characterized via 1D, 2D NMR experiments and HRMS data. Compound **6** was isolated at *m/z* 469.3314 as a white solid from the most active fraction III. A molecular formula $[C_{30}H_{44}O_4+H]^+$, having nine degrees of unsaturation, was indicated by ions observed in the HRMS experiment, which was 16.1012 Da less than beddomeilactone and equivalent to one oxygen atom. Upon examining the DNP database, it was evident that the genus *Dysoxylum* has only one compound documented with the molecular formula $C_{30}H_{44}O_4$, i.e. dysorone A, a tirucallane type of triterpenoid. The common ion fragments appeared to align with compound **1**, suggesting it could be a novel cycloartane triterpenoid with an extra oxygen molecule. Predictably, the up-field signals at δ_H 0.96 and δ_H 0.62 ppm validated the features of the cyclopropane ring, pointing towards a cycloartane-type triterpenoid and dismissing the potential of it being dysorone A. Further, 2D NMR data were obtained to establish the complete structure. A thorough literature review indicated that compound **6** was identical to the recently reported compound binectarilactone-A (Figure 3.20) from another species of *Dysoxylum* (Appendix Figure A.28-A.31) [92]. The article was published in January 2023, and this compound was not shown during the DNP dereplication as it is a recent publication, not yet included in the DNP database. However, binectarilactone A was isolated from the bark of *Dysoxylum malabaricum* for the first time.

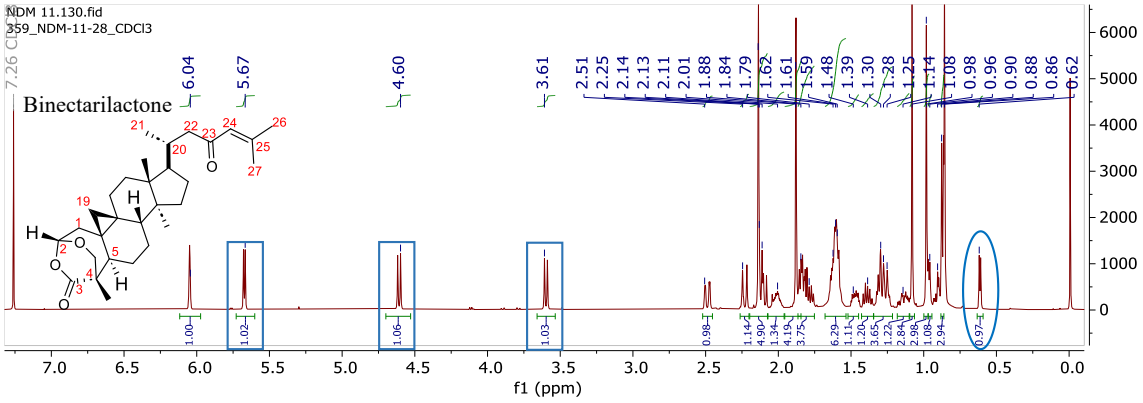

Figure 3.20. ^{1}H NMR spectrum of binectarilactone A.

Later, another mass ion peak at *m/z* 471.3459 was observed in the active fraction corresponding to the molecular formula of $C_{30}H_{46}O_4+H^+$. This compound **7** showed almost 2.0145 Da higher molecular weight than binecterilactone A (**6**). A search for DNP yielded no results; thus, compound **7** is presumed to be a new compound. Once purified, compound **7** was isolated as a white powder and assumed to be a dihydro derivative of compound **6**, having a reduced double bond with eight degrees of unsaturation. It has structural resemblances to rings A, B, C, and D from compound **6** and retains the ketone-containing side chain. Being a saturated non-polar compound, it was not detectable at short-UV wavelengths and exhibited a longer retention time during elution. Further, an in-depth structural analysis of compound **7** was conducted. Combined ^{13}C and DEPT-135 NMR confirmed six methyl, ten methylene, six methine, and seven quaternary carbons. Predictably, compound **7** showed no peaks associated with double bonds, yet extra peaks were detected in the aliphatic region. An extra CH_2 was detected at δ_C 52.7 ppm and δ_H 2.25 ppm, which was validated using DEPT-135 (Figure 3.21) and HSQC spectra (Appendix Figure A.33).

The proton signal at δ_H 2.26 ppm had a significant correlation with the carbonyl carbon at δ_C 211.2 and also with δ_C 24.6 (CH), δ_C 22.7 (CH_3), and δ_C 22.6 (CH_3). Through ^{1}H-^{1}H COSY analysis, it was confirmed that the proton at δ_H 1.47 was coupled with δ_H 0.90 (CH_3) and δ_H 1.61 (CH_3), demonstrating the presence of two terminal methyl groups

attached to methine proton at C-25.

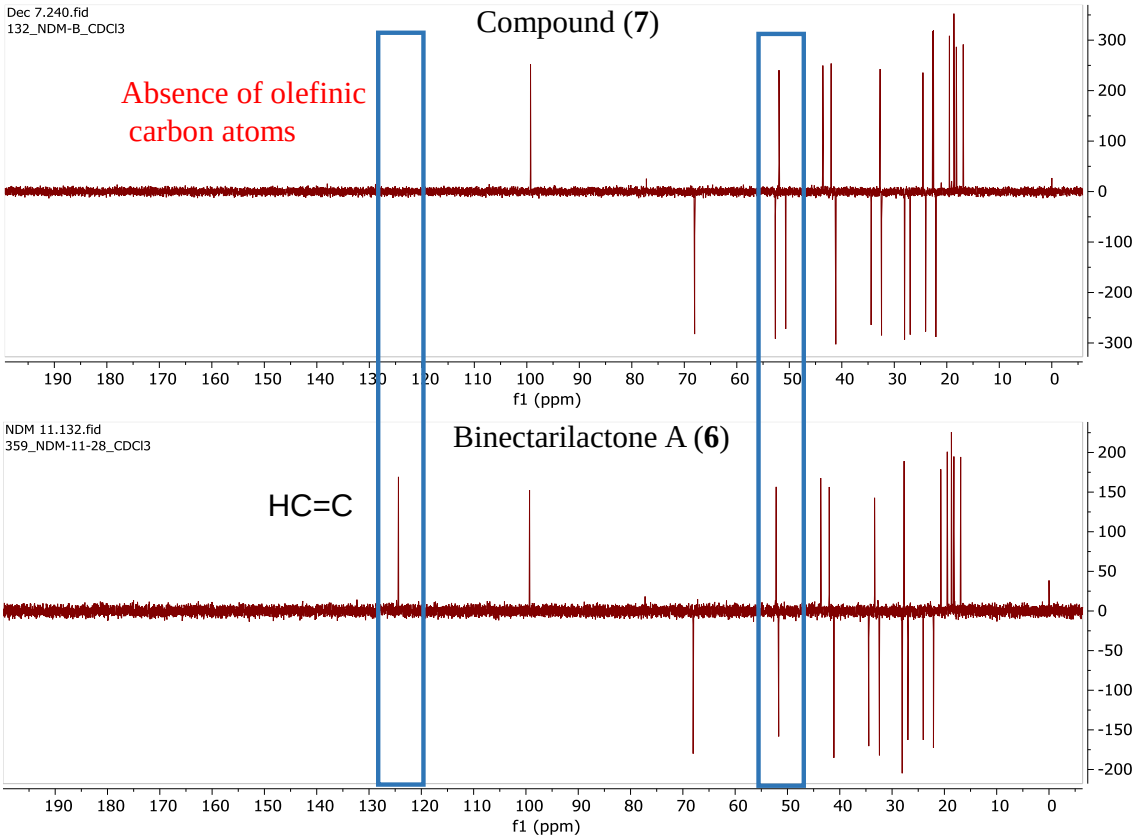

Figure 3.21. Comparative study of DEPT-135 spectra of compounds **7** and **6**.

The correlations for rings A, B, C, and D concurred and were consistent with those found in compound **6**. The relative configuration was determined by NOESY correlations between H-2a/H-29, H-16/H-24, H-24/H-27 as well as H-4/H-29 analogous to NMR results for compound **6** as shown in Figure 3.22 (a-d). Also, the NOESY correlation of ring A proposed the cis relationship between H-2 and H-29 and the co-facial orientation of the proton present in the ring system (Appendix Figure A.34). These correlations confirmed the structure of dihydrobinecterlactone A (**7**), a new metabolite. The relative configuration of the nine stereogenic centers was established as 4 S*,5 R*, 8 S*, 9 S*, 10 S*, 13 R*, 14 S*, and 17 R*.

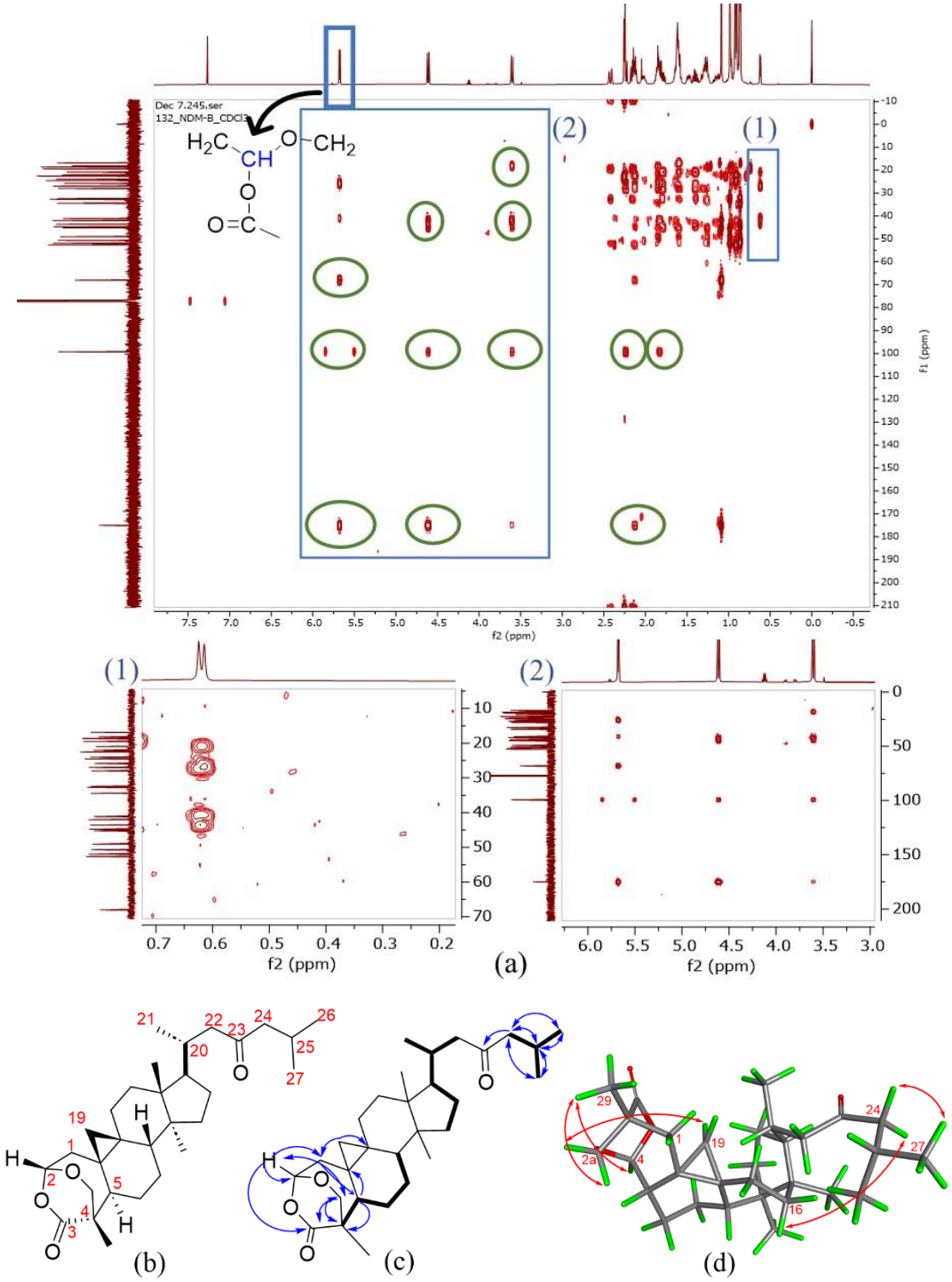

Figure 3.22. a) HMBC spectra (b) Structure (c) HMBC (↷), COSY (—) and (d) NOESY (↷) correlation of compound **7**.

The absolute configuration of compound **7** was verified through experimental ECD and compared the result with different spectra of enantiomers calculated by TD-DFT-simulated ECD experiment where mirroring of the configuration observed in compound

7 due to the structural similarities with compound **6** (Figure 3.23). The structure was confirmed as (1R,4R,5aS,6aS,8aR,9R,11aS,11bS,13aR)-4,8a,11a-trimethyl-9-(6-methyl-4-oxoheptan-2-yl)tetradecahydro-3H,6H-1,4-(epoxymethano)cyclopenta[5,6] cyclopropa[1,8a]naphtho[2,1-c]oxepin-3-one.

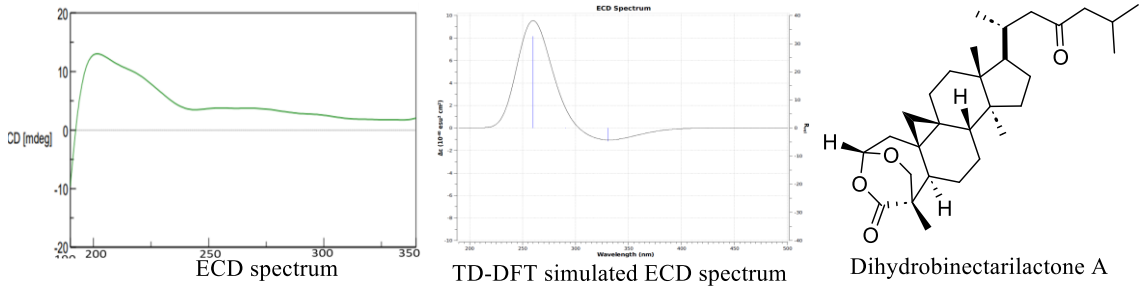

ECD spectrum TD-DFT simulated ECD spectrum Dihydrobinectarilactone A

Figure 3.23. Stereochemistry of dihydrobinectarilactone A (**7**).

Compound **8** was obtained as an off-white powder from fraction III, having a mass peak *m/z* at 492.2312 $[M+H]^+$ and a sodium adduct $[M+Na]^+$ at 513.3544. The HRMS spectra showed a molecular ion peak at *m/z* 491.3611 deduced to molecular formula $C_{30}H_{50}O_5$. Compared to compounds **6**-**7**, compound **8** exhibited greater polarity and showed no UV activity at 254 nm. The DNP search concluded that no compounds constituting 30 carbon atoms with a mass range of 490.00 to 490.999 have been reported from *Dysoxylum*. Spectral analysis showed that this new compound shared similarities with the other three isolated compounds in rings B, C, and D. However, it lacked the lactone ring A due to the occurrence of ring-opening transformation. The ^{13}C NMR and DEPT-135 NMR spectra illustrated that the structure contained seven quaternary carbons, six methyl, five methine, and twelve methylene groups. The 2D NMR data verified the fusion of the cyclopropane ring with the cyclohexane ring. In the ^1H NMR, coupled protons in the up-field linked to C19 appeared at δ_H 0.74 and δ_H 0.59 (CH_2). Two of the seven quaternary carbons were carbonyl carbons, one had a keto group at δ_C 211.9 (C23) and the other had an acid group at δ_C 184.2 (C1) as observed in Figure 3.24. A ^1H-^1H COSY correlation

was observed between the two coupled protons at δ_H 2.22 (C2) and δ_H 2.74 (C3). Both of these also displayed an HMBC correlation with the acid group positioned at δ_C 184.2 (C1). As validated by HMBC and DEPT-135, the methylene proton presents at δ_H 3.55 and δ_H 3.30 attached to δ_C 68.6 (C28b) exhibited correlation with the quaternary carbon positioned at δ_C 76.7 (C28).

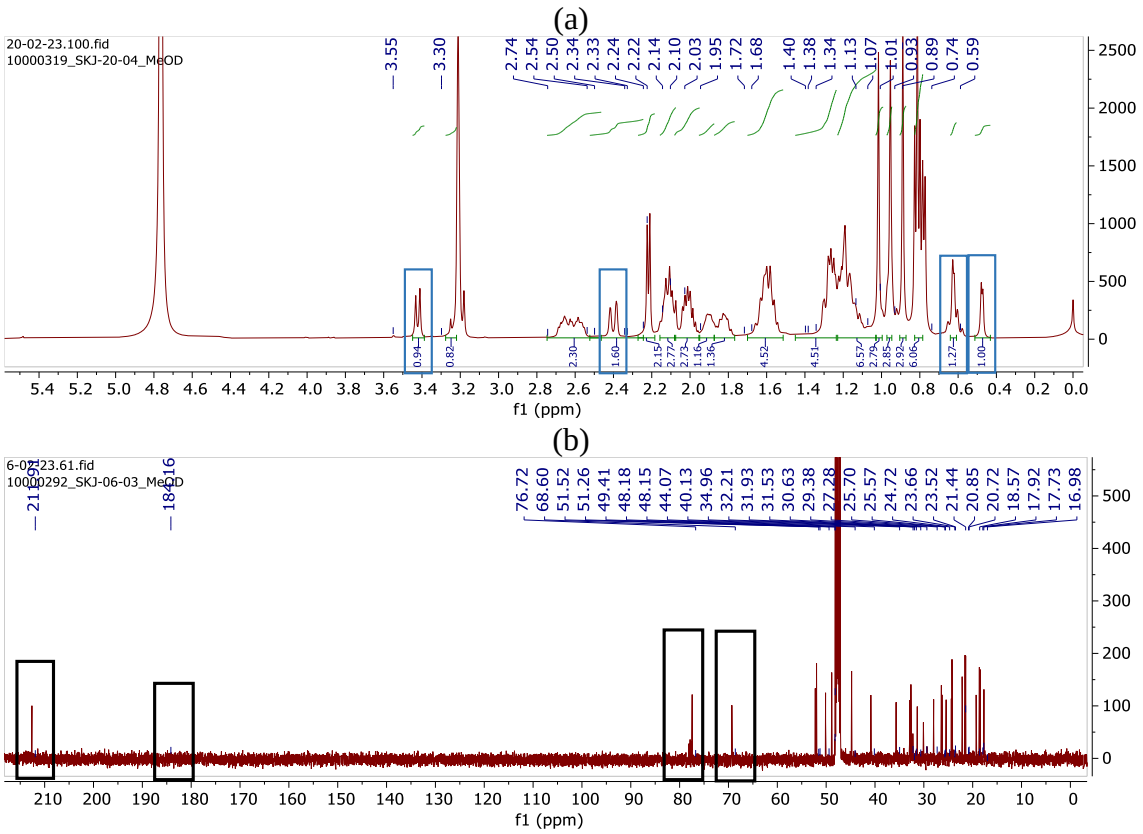

Figure 3.24. (a) ^{1}H NMR and (b) ^{13}C NMR spectra of compound **8**.

The 2D correlation data implied that hydroxy and CH_2OH groups are linked to the quaternary carbon located at δ_C 76.7 ppm (C28) (Appendix Figure A.36-A.38). However, there were no correlations found between the carbonyl carbon at δ_C 184.2 ppm (C1) and the protons on C28b (δ_C 68.6), C29 (δ_C 18.6) or C5 (δ_C 40.1). This suggests that ring A has opened. The opened configuration of ring A contains two different functionalities, one acid and two hydroxy groups at the C1 and C28 positions, and this opened structure is connected to a fused system of cyclopropane and cyclohexane, as revealed by HMBC correlations. The NOE correlations were observed between H-28b/H-6, H-19/H-11, H-

19/H-12 and H-24/H-27 (Figure 3.25). The relative configuration was determined to be 4 R*,5 S*, 8 S*, 9 S*, 13R*, 14S*, 17 R* and 28 S* showing eight stereogenic centre.

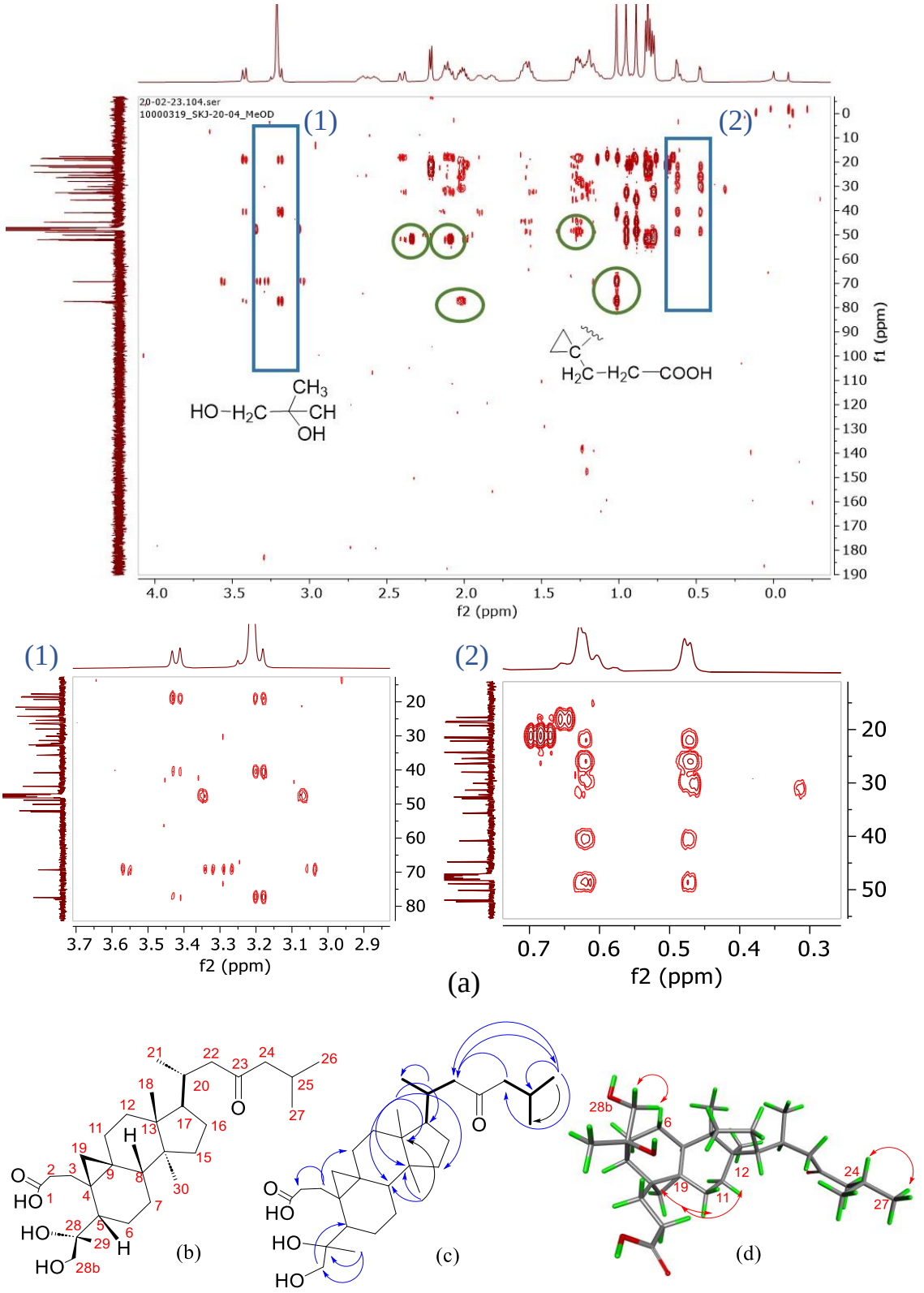

Figure 3.25. (a) HMBC spectra (b) Structure (c) Major HMBC ( ), COSY ( ) and (d) NOESY ( ) correlations of compound **8.**

Furthermore, the stereochemistry and absolute configuration were also verified by ECD experiment where the spectrum showed a good match for the above-mentioned stereogenic center with TD-DFT calculated ECD spectrum. Compound **8** showed multiple negative cotton effects as optical rotation decreases on decreasing wavelength, and two geometric minimum troughs are observed in the ECD spectra (Figure 3.26). The compound was characterized as 3-((1R,3aS,3bS,6S,6aR,7aS,9aR)-6-((S)-1,2-dihydroxypropan-2-yl)-3a,9a-dimethyl-1-(6-methyl-4-oxoheptan-2-yl)decahydro-1H-cyclopenta[a]cyclopropa[e]naphthalen-6a(7H)-yl)propanoic acid. It was named as mahamanadiol (**8)**. The NOESY correlation for ring A showed a cis relationship between H-28b, H-29, and H-5, indicating the co-facial orientation of protons attached to C28 quaternary carbon. In contrast, the trans relationship is maintained by the hydroxy and methyl group attached to carbon positioned at C28 (δ_C 76.7ppm).

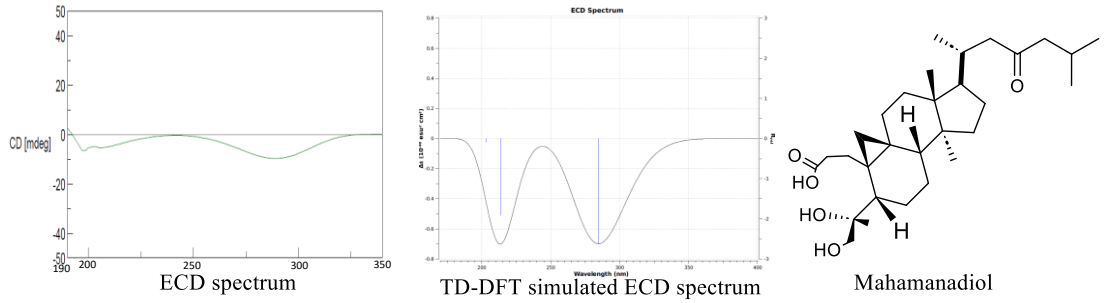

Figure 3.26. Stereochemistry of mahamanadiol (**8**).

3.3.3.2. Cytotoxicity screening of isolated compounds from fractions III

The compounds isolated from fraction III were binectarilactone A, dihydrobinectarilactone, and mahamandiol. These compounds along with mahamanlactone were evaluated against seven human cancer cell lines *viz* MCF-7 (breast carcinoma), A549 (lung epithelial carcinoma), MDA-MB-231(breast adenocarcinoma), Hs578t (breast carcinoma), ZR-75-30 (breast carcinoma), FaDU (human pharynx squamous cell carcinoma), and BT549 (breast carcinoma) for their cytotoxicity screening

using MTT assay for 48 hours to identify the most active compound. Compound **7** showed the highest cytotoxicity with IC_{50} 14 µM against the MCF-7 cell line. It was observed from the MTT assay that compounds **7** and **8** showed moderate cytotoxicity and exhibited IC_{50} in the 15-51 µM range against MDA-MB cell lines. Also, the cytotoxicity result revealed that the MCF-7 cancer cell line is the most sensitive among the panel of cell lines evaluated against the isolated compounds. The positive drug group included Paclitaxel, which showed IC_{50} 80nM for MCF-7 cell lines in this study.

3.3.3.3. Microscopic assessment of nuclear morphology

The changes in cell morphology were observed under bright-field microscopy images shown in Figure 3.27 (a), indicating cell deaths. Using fluorescence microscopy, DAPI staining with dihydrobinectarilactone (**7)** for 48 hours was performed. Cells in the control group remained intact, while the nuclear morphology of MCF-7 cells treated with dihydrobinectarilactone was altered upon treatment. The blue fluorescence of DAPI staining showed the condensation of chromatin fibers, nuclear fragmentation, and nuclear margination, indicating cell death. The number of apoptotic bodies increased with increased concentration of the compound in MCF-7 cells. The changes observed are marked in Figure 3.27 (b). The morphological changes in MCF-7 cells were also observed by evaluating intracellular ROS (Reactive Oxygen Species) generation where compound **7** treated cells showed stress releasing more ROS. The microscopic images suggested an increase in ROS generation in the treated cell compared to the control. The dichlorofluorescein (dye) fluorescence level significantly increased in the treatment group than observed in the control as shown in Figure 3.27 (c).

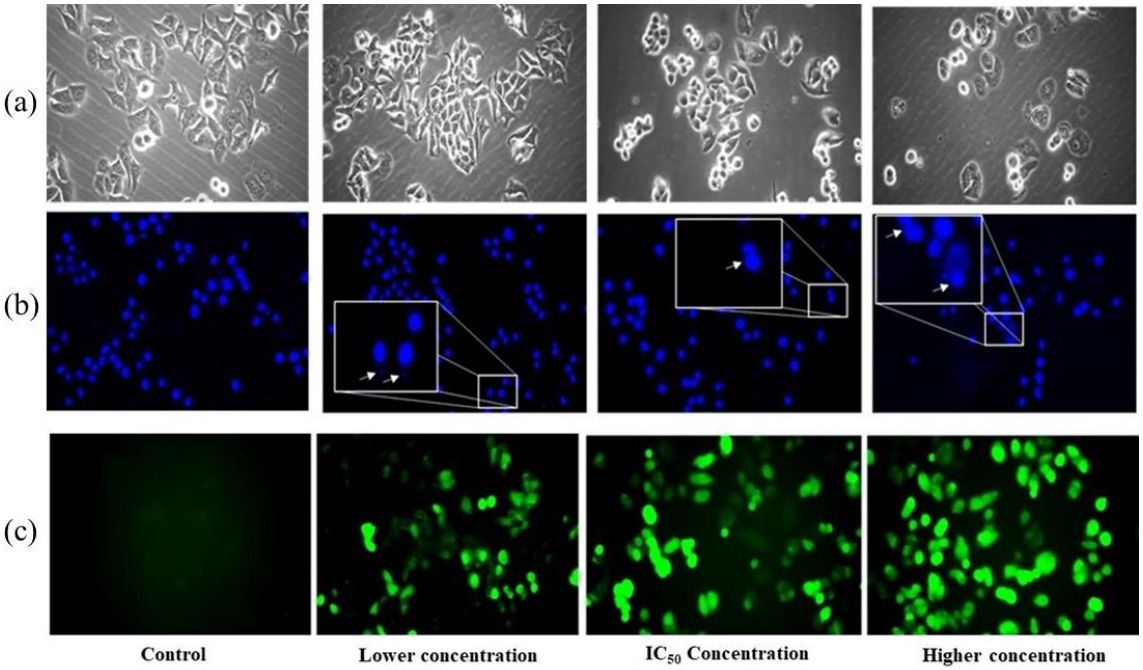

Figure 3.27. Morphological changes in MCF-7 cells after treatment with dihrdobinectarilactone A using a) Bright field image, b) DAPI staining and c) DCFDA staining (scale bar 10µm)

Similarly, the changes in cellular morphology were evaluated via acridine orange staining in the MCF-7 cell line treated with compound **7**, where an increase in lysosomes initiates cell death and thus alters the cellular processes of cancer cells (Figure 3.28).

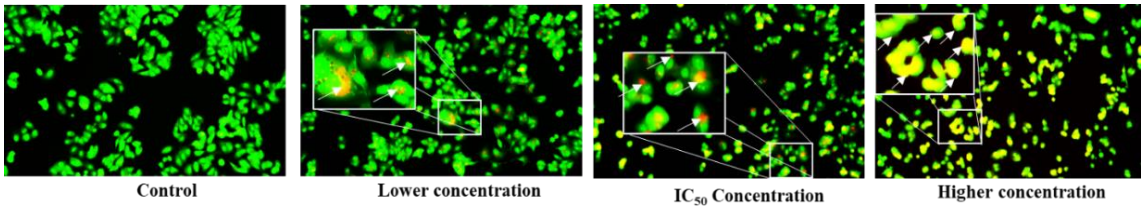

Figure 3.28. Morphological changes in MCF-7 cells after treatment with dihydrobinectarilactone A using acridine orange staining (scale bar =10µm).

3.3.3.4. Effect of dihydrobinectarilactone on cell cycle distribution of MCF-7 cells

The FACS (Fluorescence-Activated Cell Sorting) analysis was performed to determine whether the anti-proliferative action of dihydrobinectarilactone altered the cell cycle distribution profile of MCF-7 cells. The results showed a significant increase in the cell cycle arrest in the G_0/G_1 phase compared to the control group. Dihydrobinectarilactone

exhibited 81%, 85%, and 89% cell cycle arrest in G_0/G_1 phase at lower (10 µM), IC_{50}(14 µM) and higher (50 µM) concentrations, respectively, while the control group showed 61% cell cycle arrest at G_0/G_1 phase (Figure 3.29).

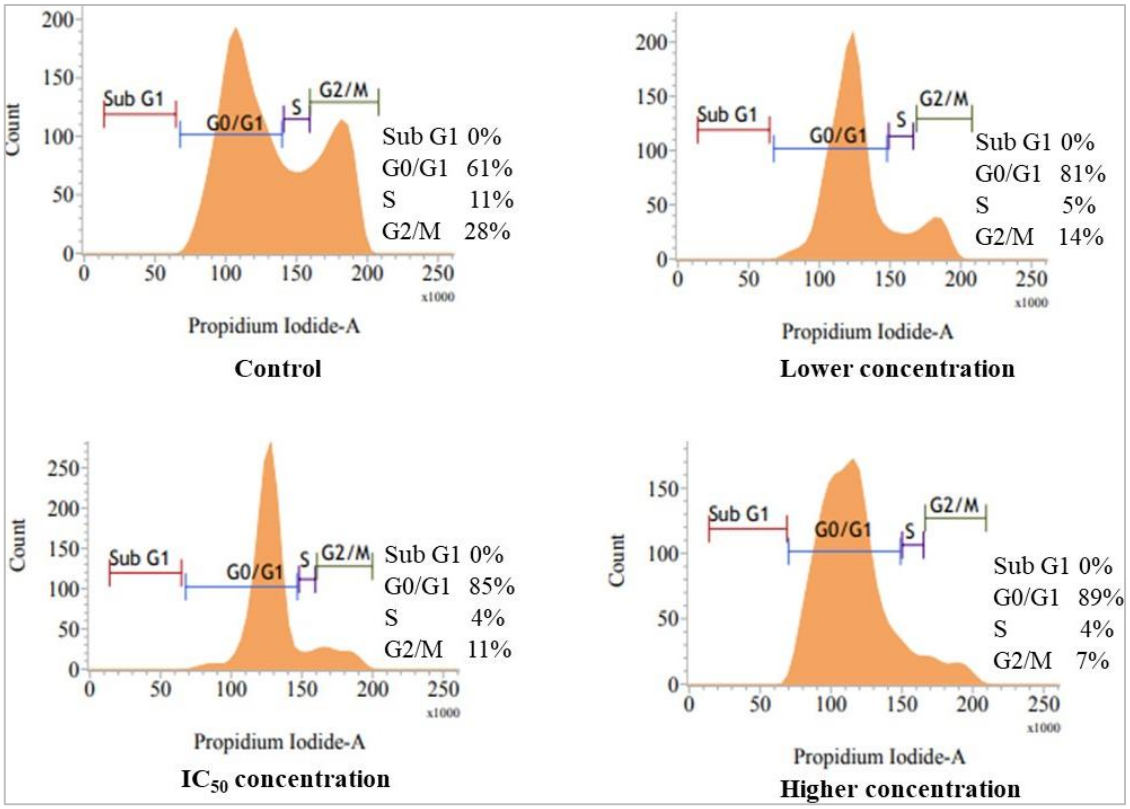

Figure 3.29. Flow cytometric analysis of treated MCF-7 cells at different concentrations of dihydrobinectarilactone A.

Furthermore, western blot analysis was performed to study the effect of dihydrobinectarilactone on the expression of various signaling proteins involved in cell cycle arrest. The expression of regulatory proteins related to different phases of the cell cycle like Cyclin B1, CDC20, CDC25, and SKP2 in MCF-7 cells was measured after treatment with dihydrobinectarilactone at lower (10 µM), IC_{50} (14 µM) and higher (50 µM) concentrations with B actin as loading control [93].

Cyclin B1, a key component in the control of cell cycle progression from G_2 to M phase, has been implicated in tumorigenesis and the development of malignancy and CDC20 appears to act as a regulatory protein interacting with many other proteins at multiple

points in the cell cycle. Cell division cycle 25 A (CDC25A), a dual-specificity protein phosphatase, is one of the most crucial cell cycle regulators, which removes the inhibitory phosphorylation in cyclin-dependent kinases (CDKs), such as CDK2, CDK4, and CDK6, and positively regulates the activities of CDKs that lead to cell cycle progression. The downregulation of CDC25 and CDC20 following the treatment with dihydrobinectarilactone for 24 hours indicates cell cycle arrest via decreased expression of these enzymes. Thus, dihydrobinectarilactone has the potential role of inhibiting these proteins in a concentration-dependent manner (Figure 3.30).

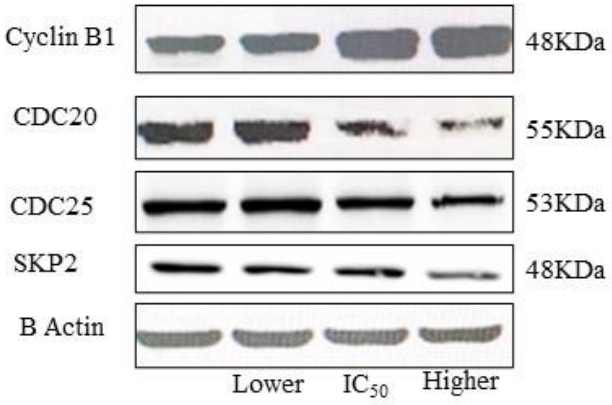

Figure 3.30. Western blot assay of MCF-7 cells showing downregulation of protein related to the cell cycle.

3.3.4. Structure elucidation and cytotoxicity screening of compounds from fraction IV

3.3.4.1. Structure elucidation of compounds targeted and isolated from fraction IV

The LCMS analysis of fraction IV showed a high-intensity peak at 9.67 and 11.55 minutes. The chromatogram at 9.67 min showed *m/z* at 513.3550. The compound was isolated as a white powder and HRMS established its mass with *m/z* 513.3553, suggesting an acetonitrile adduct. Further, based on LCMS analysis, the Chemnet DNP database was explored and expanded to target new compounds. Within the database, no triterpenoids have been reported possessing molecular weight of 472 (472.0000 to 472.9999),

accompanied by the molecular formula $C_{30}H_{48}O_4$ and featuring a basic skeleton characterized by the attachment of a cycloartane ring to an oxepanone ring. Therefore, this compound **9** was found to be new. Further, 1D and 2D NMR were carried out to elucidate the structure of compound **9**. The molecular formula of $C_{30}H_{48}O_4$ revealed 7 degrees of unsaturation deduced from the HRMS experiment. Also, the HRMS data showed a difference of 2 Da molecular weight from that of the previously isolated compound mahamanalactone A. The strong coupling of geminal proton at the highly upfield region was evident from the proton NMR spectrum, suggesting the presence of a cyclopropane ring in the structure (Figure 3.31).

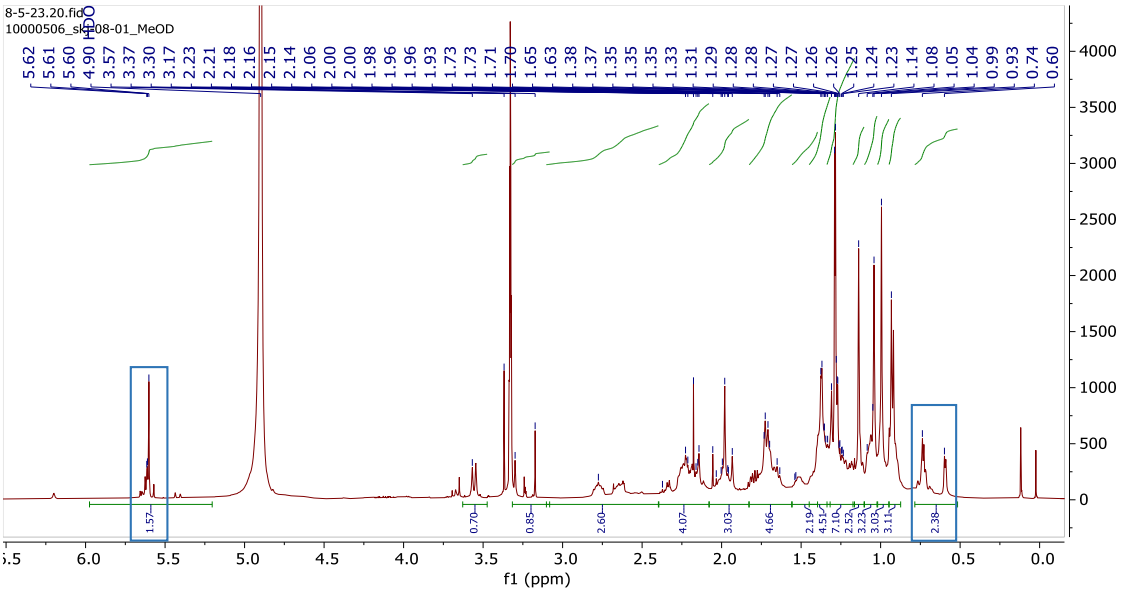

Figure 3.31. ^{1}H NMR spectrum of compound **9.**

The ^{13}C NMR spectrum showed a signal for one carbonyl carbon of cyclic ester at δ_C 174.0 and two olefinic carbon at δ_C 124.0 and δ_C 139.0. Also, the presence of vinylic proton was evident from the ^{1}H NMR spectrum at deshielded region δ_H 5.62 and δ_H 5.60. The DEPT-135 spectra revealed the presence of seven quaternary carbons, six methine and eleven methylene carbons. The spectra showed the presence of one methine group extra than mahamanalactone A (Figure 3.32).

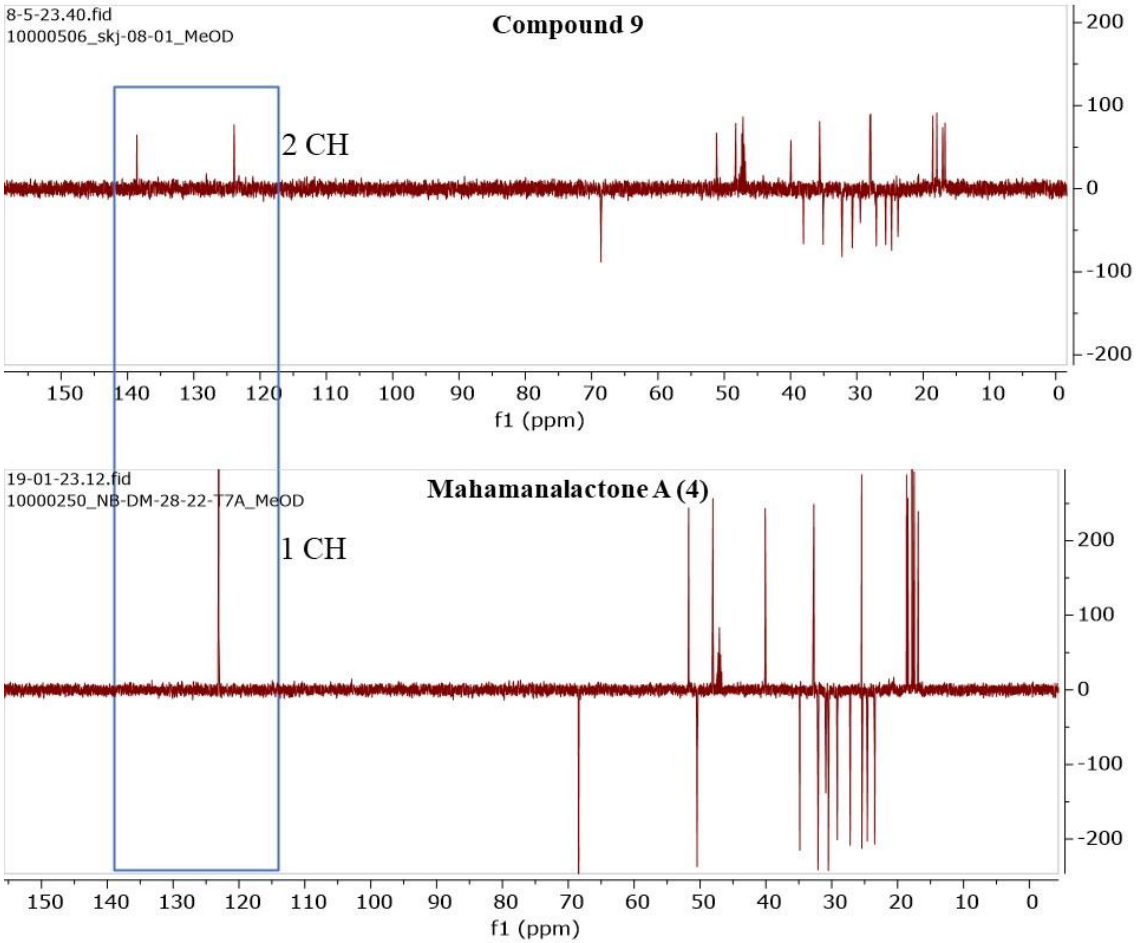

Figure 3.32. Comparative study of DEPT-135 spectra of compounds **9** and **4**.

COSY and HMBC correlation data analysis showed the presence of 7-hydroxymethyl substituted oxepan-2-one ring connected to £-caprolactone. The protons at δ_H 3.57 (C-4a, δ_C 68.6), δ_H 0.93 (C-29, δ_C 16.7) and δ_H 1.38 (C-5, δ_C 48.3) present in ring A showed a strong correlation with quaternary carbon present at C-4(δ_C 77.0) denoted by cross peaks confirming the basic scaffold of cycloartane ring as shown in HMBC spectrum. The proton at δ_H 1.35 attached to C-2 (δ_C 35.0) showed HMBC correlation with C-1 (δ_C 27.0) and the proton at δ_H 1.36 (C-1, δ_C 27.0) showed a strong correlation with C-10 (δ_C 29.5). The methyl proton at δ_H 0.99 (C-18, δ_C 18.0) correlated with C-20 (δ_C 35.6), while the methyl protons at δ_H 1.14 (C-21, δ_C 19.0) revealed correlation with C-12 (δ_C 27.1). Also, the olefinic proton at δ_H 5.60 (C-23) showed HMBC correlation with C-24 (δ_C 139.0), C-25 (δ_C 69.0) and proton at δ_H 5.62 (C-24) showed correlations with C-22(δ_C 38.0) and C-

20 (δ_C 35.6) as observed in Figure 3.33.The ^{1}H-^{1}H COSY correlation observed between H-1/H-2, H-5/H-6, H-6/H-7, H-7/H-8, H-17/H-20, H-20/H-22 and H-22/H-23. The relative configuration of compound **9** was confirmed by the NOESY experiment, where cross-peaks between H-19/H-7, H-8/H-15, H-19/H-15, H-19/H-18, H-26/H-22, H-26/H-15, H-23/H-26 were observed (Appendix Figure A.39-A.42). The stereochemistry of compound **9** was similar to our previously reported compound **4**. This new compound was named mahamanalactone C having IUPAC name (E)-9-(6-hydroxy-6-methylhept-4-en-2-yl)-1-(hydroxymethyl)-1,8a,11a-trimethyltetradecahydro-3H,6H cyclopenta [5,6] cyclopropa [1,8a] naphtho[2,1-c]oxepin-3-one.

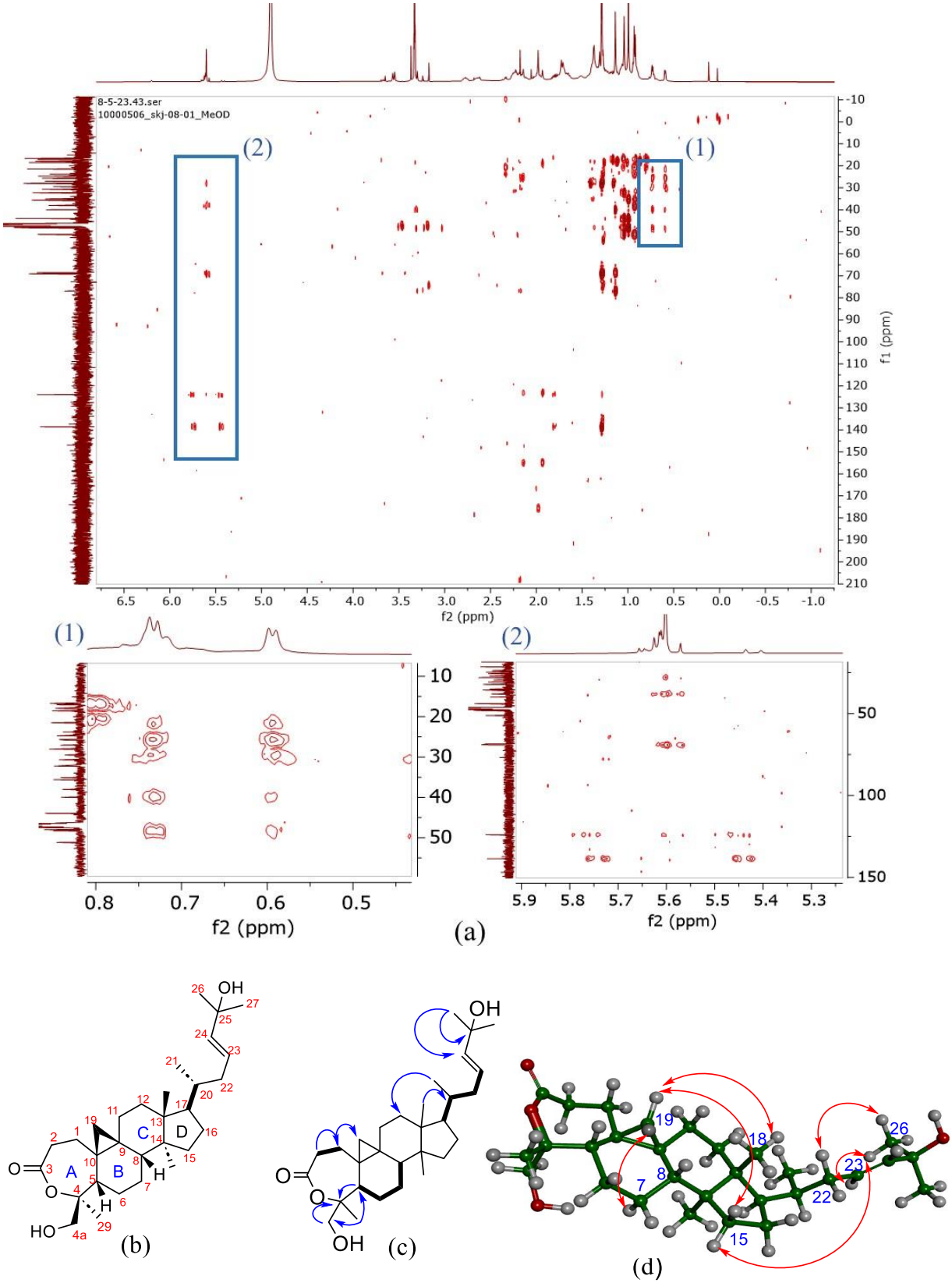

Figure 3.33. (a) HMBC spectra (b) Structure (c) Major HMBC (↷), COSY (—) and (d) NOESY (⇄) correlation of compound **9.**

Furthermore, the LCMS chromatogram at 11.55 min showed an intense peak of *m/z* 511.3386 in the bioactive fraction IV. From this fraction, compound **10** was obtained as a pale-yellow powder with HRMS spectrum showing a molecular ion peak at *m/z* 511.3378 $[M+Na]^+$ revealing a molecular formula with sodium adduct $C_{30}H_{48}O_5+Na^+$ having seven degree of unsaturation. Moreover, the HRMS data suggested a difference of 2 Da molecular weight in the structure of compound 10 and mahamanadiol. Also, the NMR spectra of compound **10** showed similarity with most of the chemical shift values of the proton as well as carbon NMR of mahamanadiol. The 1 D NMR revealed the presence of acid and ketone functionality in the basic scaffold of the compound. ^{13}C NMR and DEPT-135 spectra showed the presence of thirty carbon resonances constituting six methyl groups, eleven methylene groups, eight quaternary carbon, and five methene groups. Among them, one olefinic bond, and two carbonyl groups accounted for three indices of hydrogen deficiency, concluding that compound **10** is triterpenoid with a tetracyclic ring system (Figure 3.34). The ^1H NMR spectrum exhibited signal for six methyl protons at δ_H 1.14 (C-29, δ_C 17.9), δ_H 1.00 (C-18, δ_C 17.0), δ_H 1.06 (C-30, δ_C 17.6), δ_H 2.10 (C-21, δ_C 19.0), δ_H 1.93 (C-26, δ_C 25.7) and δ_H 0.92 (C-27, δ_C 21.2). The four-membered-ring system of compound **10** was elucidated by considering the HMBC correlation of the proton of the open ring system at H-3 (δ_H 1.74) with methylene carbon at C-2 (δ_C 33.0) and C-11 (δ_C 26.2). Also, the methyl proton at H-29 displayed two significant correlations with non-protonated carbon at C-28 (δ_C 78.9) and methylene carbon at C-28b (δ_C 68.8).

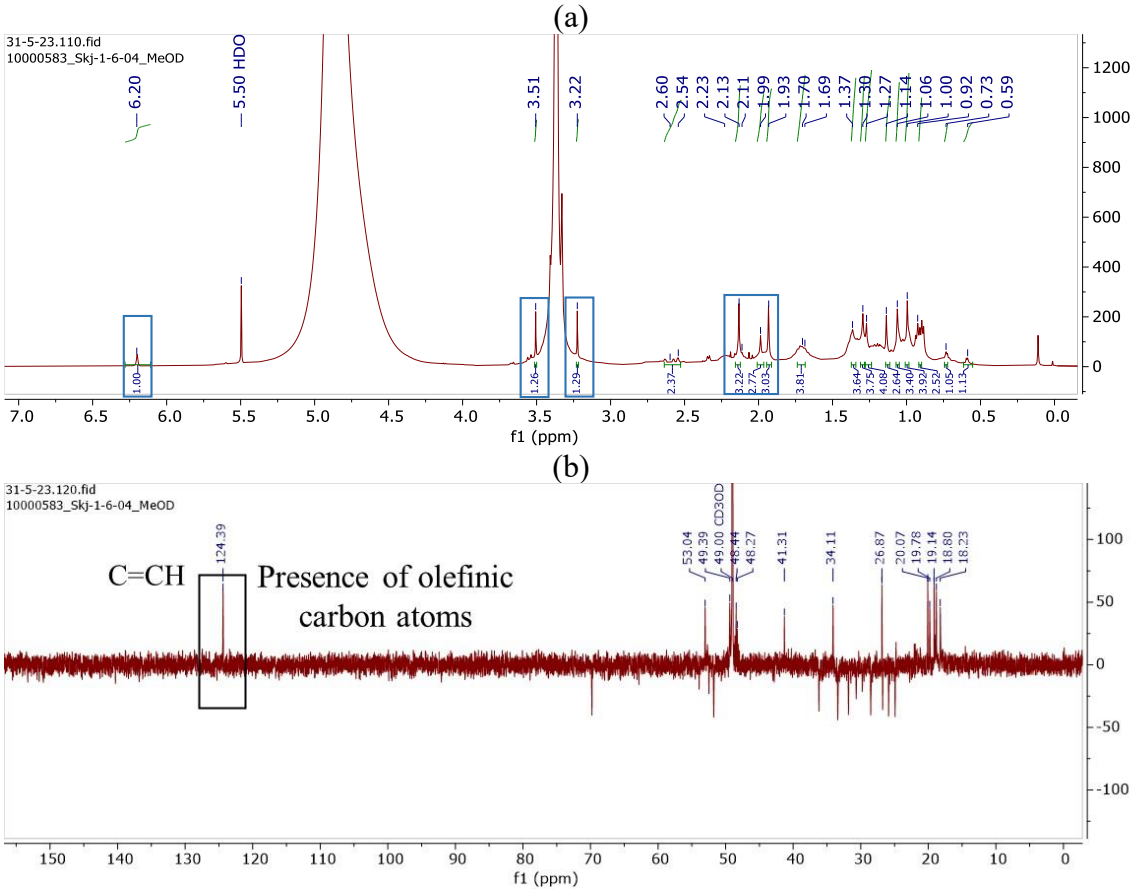

Figure 3.34. (a) ^{1}H NMR and (b) DEPT-135 spectrum of compound **10**.

The methylene proton at H-28b correlated with carbon at C-5 (δ_C 52.7). Thus, the open chain system was deduced by the HMBC spectrum (Figure 3.35). The correlation observed from methyl protons present at C-18 and C-30 with the carbon atom of B/C rings confirmed the tetracyclic structure. Also, the secondary methyl proton at C-30 correlated with C-8, C-14 and C-13. The terminal methyl proton at C-26 correlated with C-25 (δ_C 155.3), C-27 (δ_C 21.7), C-22 (δ_C 51.8) and C-24 (δ_C 123.2) along with the observed proton spin system of H-17/H-20, H-20/H-21, H-24/H-25, H-25/H-26, and H-26/H-27 from ^{1}H-^{1}H COSY spectrum suggesting the presence of a side chain attached to the ring system. The NOE spectrum revealed the cis relationship between H-28b, H-29, and H-5, suggesting the co-facial orientation of protons attached to C-28 non-protonated carbon and the trans relationship was observed by the hydroxymethyl and methyl group attached to carbon positioned at C-28 (δ_C 76.9) confirming the relative configuration of

compound **10** similar to the previously isolated compound mahamanadiol (Appendix Figure A.43-A.46). Moreover, the absolute configuration was also identical to the mahamanadiol having the same stereocentre in both structures. This isolated compound **10** was named dehydromahamanadiol.

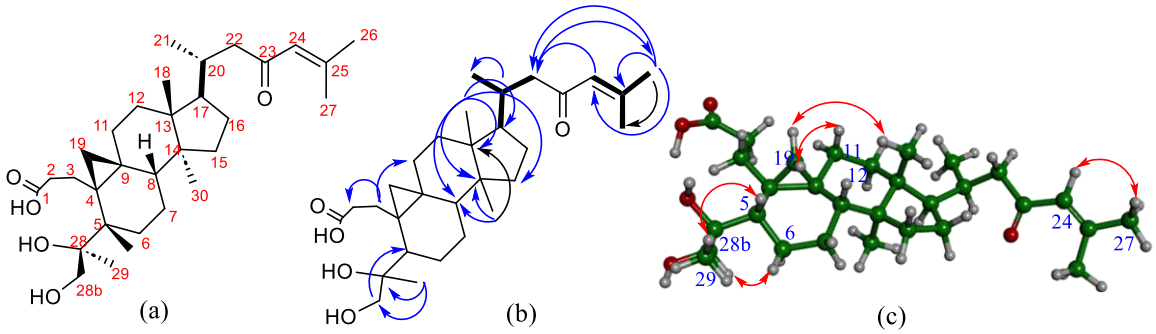

Figure 3.35. (a) Structure (b) HMBC (↷), COSY (—), and (c) NOESY (↷) correlation of compound **10.**

3.3.4.2. Cytotoxicity screening of isolated compounds from fractions IV

The ethyl acetate extract and previously isolated compounds of *D. malabaricum* demonstrated prominent cytotoxic potential against breast cancer cell lines. Triterpenoids of the cycloartane type isolated from this species have been identified to trigger apoptotic death in breast cancer cells. Therefore, compounds **9** and **10** isolated from fraction IV were evaluated for their ability to inhibit cell growth using the MTT assay on two types of human breast cancer cells: the triple-negative MDA-MB-231 and the single-positive MCF-7. The results revealed a notable cytotoxic effect that increased with concentration. Compounds **9** and **10** demonstrated considerable cytotoxic effects, with IC_{50} values of 65.01 µM and 87.99 µM, respectively, against MDA-MB-231 cells. In contrast, compounds **9** and **10** exhibited moderate cytotoxic effects against MCF-7 cells, with IC_{50} values of 149.35 µM and 157.67 µM, respectively. Hence, compound **9** exhibited more significant cytotoxicity compared to compound **10** (Figure 3.36). The isolated compounds reduced cell viability in a dose-dependent manner.

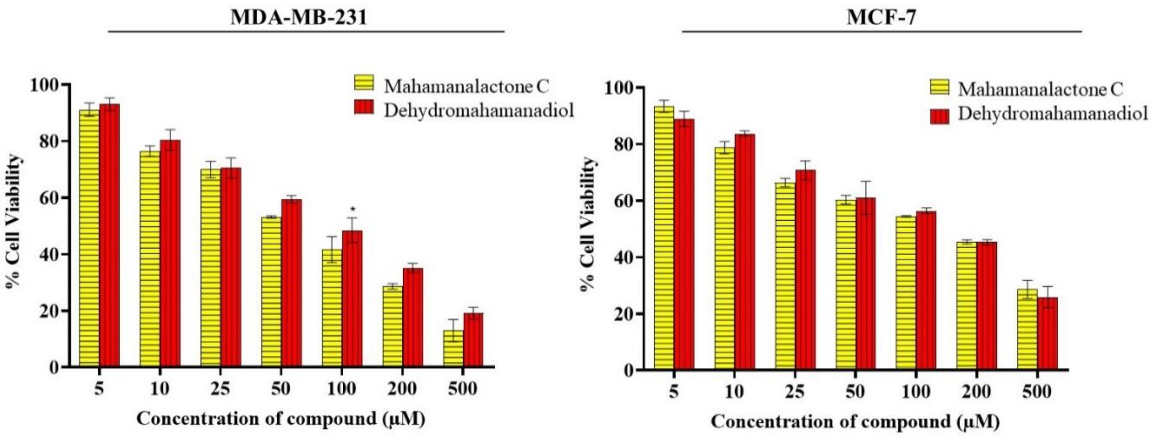

Figure 3.36. Cytotoxicity evaluation of compounds against MDA-MB-231 and MCF-7 breast cancer cells. The calculation for the p-value was done by comparing the mean ±SD of the percentage of cancer cell viability.

3.3.4.3. Glucose uptake inhibition in breast cancer cells after treatment

Glucose contributes to biomass production and controls cell signals vital for oncogenic progression and the cancer cells are more sensitive to glucose deprivation than normal cells. The administration of cytotoxic compound reduces glucose uptake, resulting in a higher concentration of glucose in the cell-free supernatant. Research findings show that blocking glucose transport can lead to apoptotic cell death and reduce cancer cell growth. The effect of isolated triterpenoids in inhibiting the proliferation of MDA-MB-231 cells through metabolic reprogramming was evaluated through a glucose uptake assay. The glucose concentration in the culture supernatant was determined after treating MDA-MB-231 cells with the IC_{30}, IC_{50}, and IC_{70} concentrations of compounds **9** and **10**. Both the compounds at concentrations of IC_{30}, IC_{50}, and IC_{70} displayed a dose-dependent reduction in glucose uptake by MDA-MB-231 cells. The compounds demonstrated a notable decrease in glucose uptake in comparison to the control across all tested durations and concentrations. The tested compounds significantly inhibited glucose uptake in MDA-MB-231 cells compared to a control group. A dose-dependent decrease in glucose uptake was observed in the treated breast cancer cells, as shown in Figure 3.37. The MDA-MB-231 cells, when treated with IC_{30}, IC_{50}, and IC_{70} concentrations of compound **9**, the

glucose levels in the supernatant rose to 110.371 ± 3.305 mg/dL, 134.132 ±2.58 mg/dL, and 198.089 ± 3.927 mg/dL respectively. This is in contrast to the control group, which had a glucose concentration of 88 ± 3.276 mg/dL. Likewise, after treating MDA-MB-231 cells with compound **10** at IC_{30}, IC_{50}, and IC_{70} concentrations, the glucose levels in the culture supernatant were observed to be 123.088 ± 4.626 mg/dL, 159.37 ± 4.093 mg/dL, and 185.313 ± 5.515 mg/dL, respectively. In contrast, the control group of MCF-7 cells had a glucose concentration of 109.24 ± 3.259 mg/dL in the culture supernatant.

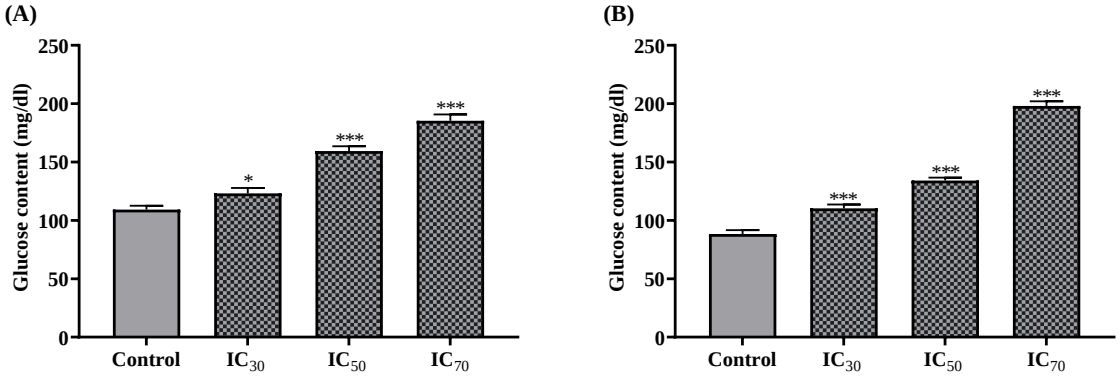

Figure 3.37. Glucose uptake inhibition in MDA-MB-231 breast cancer cells by (A) compound **9** and (B) compound **10**. The calculation for the p-value was done by comparing the mean ± SD of the concentration of glucose in control and treated cells. The statistical significance was determined using One-way ANOVA followed by the Tukey test. Statistical significance is mentioned as; ***p≤.001; **p≤.002; *p≤.033.

3.3.4.4. Enhanced Nitric oxide production in breast cancer cells after treatment

Nitric oxide (NO) is associated with processes like angiogenesis, apoptosis, cell cycle regulation, invasion, and metastasis of cancer progression. The administration of compounds **9-10** causes an increase in NO production in a concentration-dependent manner in MDA-MB-231 breast cancer cells. After treatment with compound **9** at IC_{30}, IC_{50}, and IC_{70} concentrations, the MDA-MB-231 cells showed NO levels of 14.846 ± 0.378, 16.258 ± 0.229, and 19.148 ± 0.359 µM, respectively (Figure 3.38). This is in contrast to the control, which was 13.645 ± 0.332 µM. While treatment of MDA-MB-231 cells with compound **10** at different concentrations (IC_{30}, IC_{50}, and IC_{70}) intensified the

NO production to 13.856 ± 0.314, 14.780 ± 0.380, and 17.458 ± 0.599 µM when compared to control group 13.051 ± 0.264 µM. As the concentration of the compounds increased, there was a significant rise in the amount of NO produced. NO production was significantly higher after incubation with compound **9-10** as compared to the control group, with a p-value of ≤ 0.05. At high concentrations, NO inhibits cell growth and triggers apoptosis and elevated NO production may be attributed to the activation of the i NOS gene in MDA-MB-231 cells after treatment with compound **9** and **10**.

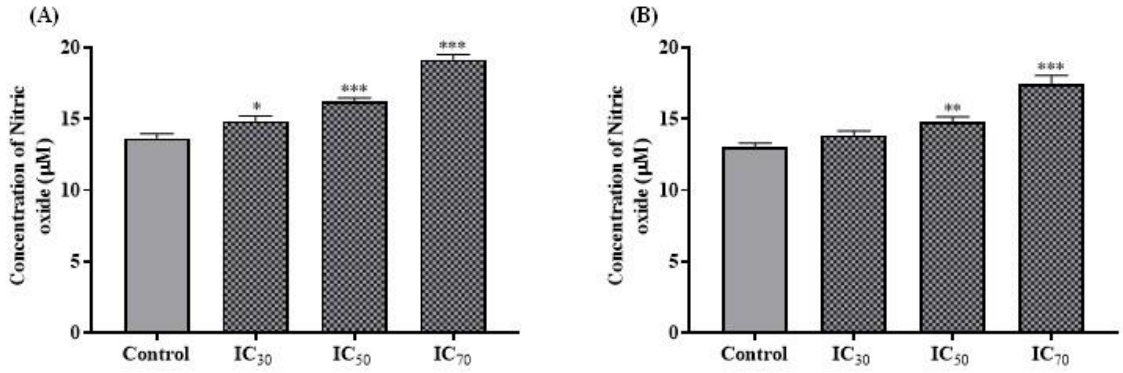

Figure 3.38. Effects of (A) compound **9** and (B) compound **10** on NO production in MDA-MB-231 breast cancer cells. The calculation for the p-value was done by comparing the mean ± SD of the level of NO in control and treated cells. The statistical significance was determined using One-way ANOVA followed by the Tukey test. Statistical significance is mentioned as; ***p≤.001; **p≤.002; *p≤.033.

3.3.4.5. Apoptosis cell death induced by mahamanalactone C

The change in nuclear morphology of breast cancer MDA-MB-231 cells treated with mahamanalactone C (**9)** was assessed using DAPI staining. To assess the nuclear morphological modifications after 24 hours of exposure, three different concentrations of compound **9**, namely IC_{30} (24.269 ± 4.085 µM), IC_{50} (65.015 ± 5.576 µM), and IC_{70} (188.551±6.561 µM), were evaluated on MDA-MB-231 cells. At higher concentrations (IC_{70}), compound **9** induces significant morphological changes in breast cancer cells. Fluorescence imaging characterized these changes as notably nuclear pyknosis compared

to cells treated with lower concentrations. The arrow present in the images of treated cells indicates signs of abnormal cell morphology, chromatin condensation, nuclear distortion, and disintegration (Figure 3.39). The control group with MDA-MB-231 cells exhibited regular cell shapes and undamaged nuclei [94].

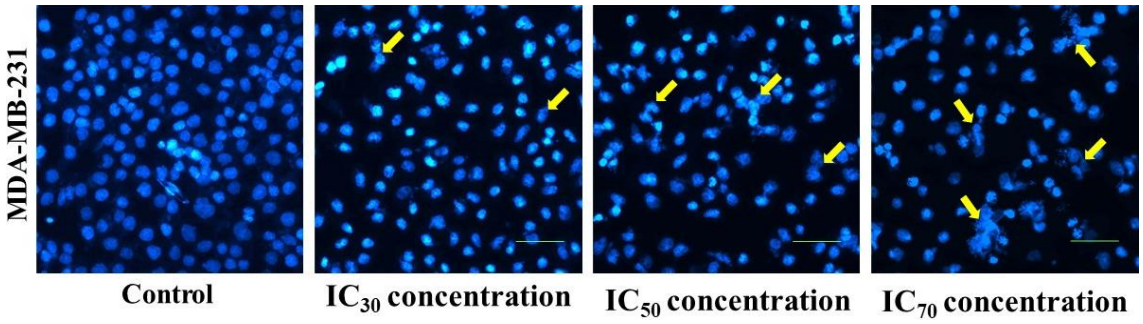

Figure 3.39. Morphological changes in MDA-MB-231 cells after treatment with dehydromahamanadiol (scale bar 10µm).

3.4. Outcomes

The study demonstrated the application of LC-MS to identify new compounds from the bark extract of *D. malabaricum* by applying different spectral information and using the DNP chemical database. The crude extract was subjected to bioassay-guided fractionation followed by LC-MS analysis for isolation of compounds. The LC-MS profiling effectively detected the new triterpenoids in the ethyl acetate active fraction. Further, the targeted compounds were subjected to isolation using repeated silica-gel-based column chromatography and HPLC. The study resulted in the isolation of fourteen triterpenoids. Ten cycloartane type triterpenoids were first time isolated from *D. malabaricum.* Other than cycloartane type triterpenoid stigmasterol, sitosterol, campesterol, and lupeol were isolated from the bark extract. Eight new compounds named dihydrobeddomeilactone, hydroxybeddomeilactone, mahamanalactone A, dihydromahamanalactone A, dihydrobinectarilactone, mahamanadiol, mahamanalactone C, dehydromahamanadiol were isolated (Figure 3.40). *Dysoxylum malabaricum* has proven to be a new source of cycloartane triterpenoids. The structure and stereochemistry of the new compounds were

identified by spectral techniques and the compounds were evaluated for their cytotoxic potential against breast cancer cell lines viz T-47D, MDA-MB-231, MCF-7, BT-549, Hs-578t and ZR-75-30. The cycloartane triterpenoids induced altered cell morphology and showed signs of apoptotic cell death in breast cancer cells after treatment. Further *in-vitro* cytotoxic potential of dihydrobinectarilactone was investigated on MCF-7 cells in detail where this triterpenoid causes cell cycle arrest of MCF-7 cells via downregulation of CDC20 and CDC25 enzymes.

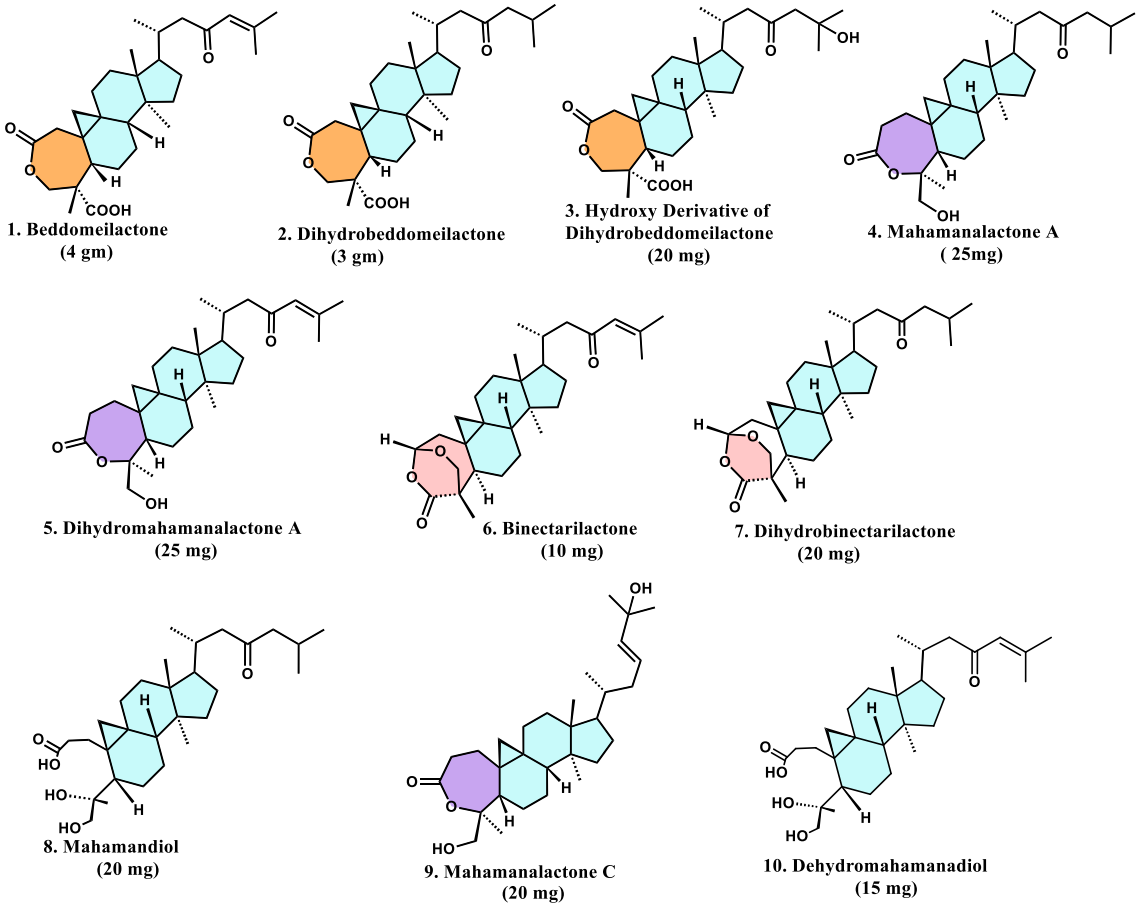

Figure 3.40. Structures of isolated cycloartane triterpenoids from bark extract.